

Investigating two-dimensional adjoint QCD on the lattice

Georg Bergner^a Stefano Piemonte^b Mithat Ünsal,^c

^a*University of Jena, Institute for Theoretical Physics,
Max-Wien-Platz 1, 07743 Jena, Germany*

^b*University of Regensburg, Institute for Theoretical Physics,
Universitätsstr. 31, 93040 Regensburg, Germany*

^c*Department of Physics, North Carolina State University, Raleigh, NC 27695, USA*
*E-mail: georg.bergner@uni-jena.de, stefano.piemonte@ur.de,
unsal.mithat@gmail.com*

ABSTRACT: We present our investigations of $SU(N)$ adjoint QCD in two dimensions with one Majorana fermion on the lattice. We determine the relevant parameter range for the simulations with Wilson fermions and present results for Polyakov loop, chiral condensate, and string tension. In the theory with massive fermions, all observables we checked show qualitative agreement between numerical lattice data and theory, while the massless limit is more subtle since chiral and non-invertible symmetry of the continuum theory are explicitly broken by lattice regularization. In thermal compactification, we observe N perturbative vacua for the holonomy potential at high- T with instanton events connecting them, and a unique vacuum at low- T . At finite- N , this is a cross-over and it turns to a phase transition at large- N thermodynamic limit. In circle compactification with periodic boundary conditions, we observe a unique center-symmetric minimum at any radius. In continuum, the instantons in the thermal case carry zero modes (for even N) and indeed, in the lattice simulations, we observe that chiral condensate is dominated by instanton centers, where zero modes are localized. We present lattice results on the issue of confinement vs. screening in the theory and comment on the roles of chiral symmetry and non-invertible symmetry.

Contents

1	Introduction	1
2	Overview of continuum theory on \mathbb{R}^2	3
2.1	Confinement vs. screening	4
2.2	Vacuum degeneracy, universes vs. ordinary vacua	6
2.3	On $\mathbb{R} \times S^1$, with periodic and anti-periodic boundary conditions	7
2.4	Instantons in the thermal case	9
2.5	Chiral symmetry on $\mathbb{R} \times S^1$	11
3	Observables on the lattice	14
3.1	Polyakov loop related observables	15
3.2	Instantons and chiral condensate at high-temperature	19
3.3	Zero temperature fermion condensate	20
3.4	String tension	21
3.5	Lightest fermion and boson states	25
4	Conclusions and future directions	26
A	Theory on the lattice	28
A.1	Lattice action and algorithms	28
A.2	Parameter tuning	29
B	Further results	30

1 Introduction

Perhaps, the two most dramatic differences between the two-dimensional and four-dimensional QCD with one massless adjoint Majorana fermion [QCD(adj)] are the following. Classically, the static test charges in the two-dimensional model interact via a (confining) linear Coulomb interaction leading to a potential $V(r) \sim r$ while quantum mechanically, it is expected that $V(r) \sim (1 - \exp(-Mr))/M$, and the theory is in deconfined Higgs phase [1]. In contradistinction, the test charges in the four-dimensional model interact via Coulomb interaction $V(r) \sim 1/r$ while quantum mechanically, it is expected that $V(r) \sim \sigma r$, and the theory is in a confining phase [2]. In other words, the four-dimensional theory, which is not confining classically, becomes confining quantum mechanically and two-dimensional theory, which is confining classically, becomes non-confining quantum mechanically.

The other strange aspect of massless 2d $SU(N)$ QCD(adj) relative to the corresponding four-dimensional theory is its ground state degeneracy and relatedly its global symmetry. The standard global symmetry in these two cases is rather similar, but the two-dimensional theory also possesses a non-obvious global symmetry, called non-invertible symmetry [3]. The respective symmetries for $n_f = 1$ flavor theories are

$$G = \begin{cases} \left[\mathbb{Z}_N^{[1]} \rtimes (\mathbb{Z}_2)_C \right] \times (\mathbb{Z}_2)_F \times (\mathbb{Z}_2)_\chi \times G_{\text{non-inv}} & \text{2d massless QCD(adj)} \\ \left[\mathbb{Z}_N^{[1]} \rtimes (\mathbb{Z}_2)_C \right] \times (\mathbb{Z}_2)_F \times (\mathbb{Z}_{2N})_\chi & \text{4d massless QCD(adj)} \end{cases}, \quad (1.1)$$

while the respective number of vacua are given by

$$\mathcal{N}(\text{vacua}) = \begin{cases} 2^{N-1} & \text{2d massless QCD(adj)} \\ N & \text{4d massless QCD(adj)} \end{cases} . \quad (1.2)$$

While the slight change in the discrete chiral symmetry is due to nature of Majorana fermion in 2d vs. 4d, the exotic vacuum degeneracy is dictated by representations of the non-invertible symmetry.¹

These two facts should make it clear that the goal of studying QCD(adj) in two dimensions is not necessarily to have a simpler toy model for the dynamics of a strongly coupled four-dimensional theory. Rather, one sensible goal is to gain a deeper and broader understanding of quantum gauge theories and their possible behaviors.

In two-dimensional pure Yang-Mills theory, there are effectively no dynamical gauge degrees of freedom, and both classical and quantum theory exhibit linear confinement, as it can be shown by analytical methods [4]. The theories become non-trivial as soon as bosonic or fermionic matter fields are added. The situation with $SU(N)$ QCD(adj), or Yang-Mills with one Majorana fermion is rather special as described above. As explained, the exactly massless theory with standard fermion term $\text{tr}[\bar{\psi}\gamma_\mu D_\mu\psi]$ is non-confining, a surprising behaviour as pointed out in [1]. For a more general perspective, we have to consider additional deformations by other operators. Once a chiral symmetry breaking mass term is turned on, the theory becomes confining. However, about twenty-five years after this first analysis, it has been understood that two-dimensional QCD(adj) (QCD₂(adj)) admits certain classically marginal four-fermion deformations [5], just as the Gross-Neveu model [6], which can become relevant in the quantum theory [7]. The result of [5] is based on mixed anomalies between the standard symmetries of the system, as well as the notion of adiabatic continuity and semi-classical limit in exact agreement with anomalies. These deformations make the massless theory confining for all representations (except for N -ality $N/2$ for even N), proving that the mass term is not the only deformation inducing confinement in this theory.

Motivated by the combination of the results of [1] and [5], Ref. [3] made a further significant progress. It showed that the massless QCD₂(adj) with just standard fermion terms $\text{tr}[\bar{\psi}\gamma_\mu D_\mu\psi]$ has an extra global symmetry, called non-invertible symmetry, $G_{\text{non-inv}}$. The practical utility of this symmetry is that it forbids the four-fermion deformations which are allowed by standard global symmetries.

The four-fermion operators are meant to be for the non-invertible symmetry what the mass operator is for chiral symmetry. These operators are charged under the respective symmetry, but we are free to study the behaviour of the theory by turning them on. Indeed, Ref. [3] studied the response of the theory by turning on four-fermion deformations and reached to the same conclusion as [5], that all representations except for N -ality $0, N/2$ exhibit confinement. This result actually tells us that [1] and [5] are not conflicting with each other. Some other work on QCD₂(adj) can be found in [3, 5, 7–17].

We now understand that an analogous, but relatively simpler story holds in charge- q version [18–22] of Schwinger model [23]. It is usually asserted that Schwinger model with massless fermions always exhibits screening, while its massive deformation confines. These statements have a precise meaning in the charge- q version which possess a $\mathbb{Z}_q^{[1]}$ 1-form symmetry. However, a four-fermion deformation of the Schwinger model, which respects a \mathbb{Z}_4 subgroup of \mathbb{Z}_{2q} chiral symmetry, which is large enough to prohibit a mass term for $q = \text{even}$, is shown to be confining if the four-fermion deformation is relevant [24], mimicking the story in QCD₂(adj).

The present work is an initial study to explore some of the interesting dynamics of QCD₂(adj) by using lattice gauge theory, a manifestly non-perturbative framework. For the evaluation of finite

¹Furthermore, to add more to the strangeness of 2d theory, these 2^{N-1} vacua are split to N universes, sectors which are separated by *non-dynamical* domain-walls, charged under 1-form symmetry. Each universe supports about $2^{N-1}/N$ vacua separated by standard dynamical domain walls. We review this structure in Sec. 2.2.

temperature chiral condensate and Polyakov loop properties, we use Wilson fermions. To evaluate the zero temperature chiral condensate, we use overlap fermions by reweighting. Lattice formulation proved to be very useful for the investigation of QCD and Yang-Mills theories in \mathbb{R}^4 by simulating the theories on large discretized torus T^4 . In two dimensions these well-established methods also provide important cross-checks and insights. The lattice studies of two-dimensional gauge theories have so far mainly considered the Schwinger and 't Hooft models [25, 26]. Some very preliminary studies exist also for the case of adjoint QCD in two dimensions [27]. Recently, an interesting alternative approach using a lattice Hamiltonian formulation has been applied in the case of $SU(2)$ [15]. Some related supersymmetric gauge theories have been already investigated on the lattice in some numerical studies [28, 29]. In addition, two-dimensional gauge theories have been an ideal playground to test numerical methods, algorithms, and approaches.

The main results of our numerical simulations, which always approach the theory from a finite mass regime, are the following. In thermal case, absolute value of the Polyakov loop makes a cross-over from small $|\text{tr } P|$ towards $|\frac{1}{N} \text{tr } P| \sim 1$ at some $T_c \sim g$. At high- T , we find N vacua and tunnelings (instanton events) connecting them. Due to tunnelings, $\langle \text{tr } P \rangle = 0$ in both phases and strictly speaking, there is no phase transition at finite- N . In circle compactification with periodic boundary conditions, we observe a unique vacuum for Polyakov loop, i.e. small $|\text{tr } P|$ even at small circle with global minimum of the effective potential around $\text{tr } P = 0$. We determine a chiral condensate at low and high temperature. The high-temperature condensate is dominated by the instanton events interpolating between the N vacua. Concerning confinement vs. screening, at finite values of m , we observe a finite string tension. In the chiral limit, the tension tends to zero consistent with screening. Note, however, that our simulations may not be precise enough to capture the effects of four-fermion induced confinement.

The paper is organized as follows: In Sec. 2, we first overview briefly what is known about the continuum theory on \mathbb{R}^2 and $\mathbb{R} \times S^1$, both in thermal and circle compactification suitable for adiabatic continuity. We apply quite standard techniques for the simulations of the theory and therefore only a short discussions of the methods is presented in Sec. A. Since the theory is distinguished from four dimensional counterparts, we provide a longer discussion of the relevant parameter range and tuning in Sec. A.2. In Sec. 3, we present data for the observables of the theory, showing the zero temperature and finite temperature fermion condensates, Polyakov loop, its modulus and susceptibility as observables. In order to provide a careful study of the confinement properties, we present different methods to estimate the string tension in Sec. 3.4. Finally we discuss some preliminary results on the lightest boson and fermion masses.

2 Overview of continuum theory on \mathbb{R}^2

We are considering $SU(N)$ Yang-Mills theory in two dimensions coupled to an adjoint Majorana fermion (QCD₂(adj)). The Lagrangian of this theory is²

$$S = \int d^2x \frac{1}{2g^2} \text{tr}[F_{\mu\nu}F_{\mu\nu}] + \text{tr}[\bar{\psi}(\gamma_\mu D_\mu)\psi], \quad (2.1)$$

with gauge field strength $F_{\mu\nu}^a$ and a Majorana fermion ψ in the adjoint representation. Instead of the gauge coupling g , we can also use the 't Hooft coupling $\lambda = g^2 N$. D_μ is the covariant derivative.

Massless QCD₂(adj) possesses ordinary 0-form, 1-form, and non-invertible symmetries, which makes their interplay quite interesting. As explained, the complete symmetry group is in this case

$$G = \left[\mathbb{Z}_N^{[1]} \rtimes (\mathbb{Z}_2)_C \right] \times (\mathbb{Z}_2)_F \times (\mathbb{Z}_2)_\chi \times G_{\text{non-inv}}. \quad (2.2)$$

²The conventions for the Euclidean γ matrices $\gamma_0 = \sigma_1$; $\gamma_1 = -\sigma_2$, which means $\gamma_* = \gamma_3 = i\gamma_0\gamma_1 = \sigma_3$. The charge conjugation matrix is $C = \gamma_1$. 0 direction corresponds to x (length $\tilde{L} = L_x$), 1 direction corresponds to t (length $L = L_t = 1/T$). t is the direction of thermal/periodic compactification.

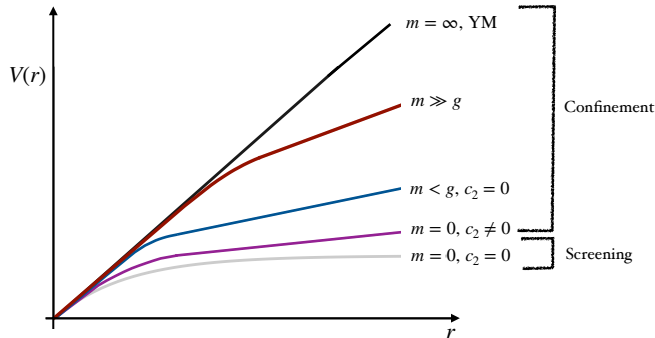


Figure 1: Cartoon of potential between test charges in a generic representation in $SU(N)$ QCD(adj) $N \geq 3$. The theory is in the screening phase if $(\mathbb{Z}_2)_\chi \times G_{\text{non-inv}}$ breaking perturbations are turned off, $m = 0, c_2 = 0$. Turning on either perturbations leads to confinement except for the N -ality $N/2$ in the case of $c_2\mathcal{O}_2$ deformation. The relatively new realization is that exactly massless theory becomes confining with the c_2 deformation as shown by using mixed anomalies and explicit soft breaking of non-invertible symmetry. At infinite mass limit, the tensions are representation dependent rather than N -ality. The change in slope for $m \gg g$ is a transition from a representation dependent tension to N -ality dependent tension.

The theory admits a relevant mass deformation and two marginally relevant four-fermion deformations:³

$$\begin{aligned}
 m\mathcal{O}_\chi &= m \operatorname{tr}[\bar{\psi}\psi] && \text{breaks } (\mathbb{Z}_2)_\chi \times G_{\text{non-inv}} \\
 c_1\mathcal{O}_1 + c_2\mathcal{O}_2 &= c_1 \operatorname{tr}[\bar{\psi}\gamma_\mu\psi\bar{\psi}\gamma_\mu\psi] + c_2 \operatorname{tr}[\bar{\psi}\psi] \operatorname{tr}[\bar{\psi}\psi], && \text{breaks } G_{\text{non-inv}}.
 \end{aligned} \tag{2.3}$$

Since the canonical dimension of fermions in two dimensions is $[\psi] = 1/2$, it is natural to consider these four-fermion deformations as proposed in [5]. These operators are classically marginal, i.e. their coefficients are dimensionless. These four-fermion operators respect all standard (invertible) symmetries, but \mathcal{O}_2 violates the non-invertible symmetry. One can show that the coupling constants are asymptotically free for a certain choice of the couplings, [7], just like in the Gross-Neveu model [6], hence the operator is marginally relevant and alters the IR dynamics.

It has been shown in Ref. [3] that non-invertible symmetry $G_{\text{non-inv}}$ forbids the dangerous one of these four fermion operators, \mathcal{O}_2 , just like chiral symmetry $(\mathbb{Z}_2)_\chi$ forbids the mass operator. Therefore, in a microscopic regularization which respects $G_{\text{non-inv}}$, these operators are not generated and one can set their coefficients consistently to zero. However, if regularization does not respect $G_{\text{non-inv}}$, these operators are generically generated, and their effects can alter the IR dynamics.

2.1 Confinement vs. screening

The feature that makes QCD₂(adj) a rather interesting theory is the fact that the explicit breaking of either of the $(\mathbb{Z}_2)_\chi$ and/or $G_{\text{non-inv}}$ symmetries changes the dynamics drastically. Note that an $(\mathbb{Z}_2)_\chi$ breaking perturbation also necessarily breaks $G_{\text{non-inv}}$. However, the inverse is not true. The four-fermion deformation considered above breaks $G_{\text{non-inv}}$, but respects $(\mathbb{Z}_2)_\chi$. The resulting outcomes on \mathbb{R}^2 are the following:

³The mapping to chiral basis is as follows: $\mathcal{O}_\chi = \operatorname{tr}[\psi_+\psi_-]$, $\mathcal{O}_1 = \operatorname{tr}(\psi_+\psi_+\psi_-\psi_-)$, $\mathcal{O}_2 = \operatorname{tr}(\psi_+\psi_-) \operatorname{tr}(\psi_+\psi_-)$.

- Classically, the theory with $(\mathbb{Z}_2)_\chi \times G_{\text{non-inv}}$ symmetry ($m = 0, c_2 = 0$) has a linear Coulomb potential among test charges, but quantum mechanically, it is deconfined. The quantum theory has an exponentially large number of vacua, 2^{N-1} , half bosonic and half fermionic.
- A mass deformation of the theory, $m \neq 0$, explicitly breaking both $(\mathbb{Z}_2)_\chi \times G_{\text{non-inv}}$, leads to confinement, with a string tension $\sigma \sim mg$ at long distances. The vacuum is expected to be unique.
- A four-fermion deformation which explicitly breaks $G_{\text{non-inv}}$ but respects $(\mathbb{Z}_2)_\chi$ is also expected to lead to confinement, similar to four-fermion deformation of the massless Schwinger model [24]. The number of vacua is 2 for $N \neq 4n + 1$ ($n = 1, 2, \dots$), and otherwise there is a unique vacuum.
- If we explicitly break the non-invertible symmetry $G_{\text{non-inv}}$, and keep the ordinary global symmetries (2.2) intact, then the massless theory confines all representations except for N -ality 0, $N/2$, i.e.

$$\sigma_k \neq 0 \quad \text{for } k \neq 0, N/2, \quad \text{and symmetry breaking } \mathbb{Z}_N \rightarrow \mathbb{Z}_{N/2}. \quad (2.4)$$

In the $m \rightarrow \infty$ limit, $\text{QCD}_2(\text{adj})$ reduces to pure Yang-Mills theory without fermions. This is an almost topological theory without any physical degrees of freedom. This theory can be solved exactly. The string tensions can be computed exactly [4]. In the case of $\text{SU}(2)$ gauge theory, the string tension in representation $j = 1/2, 1, \dots$ is

$$\sigma_j(\beta) = -\log \left(\frac{I_{2j+1}(\beta)}{I_1(\beta)} \right) \xrightarrow{\beta \rightarrow \infty} \frac{1}{\beta} j(j+1) \equiv \frac{1}{\beta} C_2(j), \quad (2.5)$$

where $I_n(x)$ are modified Bessel functions. See Section 14 of Ref. [30] for details. The fact that string tensions are not classified under the \mathbb{Z}_2 center of $\text{SU}(2)$, but rather in terms of quadratic Casimir of the spin- j representations is explained in terms of another non-invertible symmetry. This non-invertible symmetry is a 1-form symmetry $G_{\text{non-inv}}^{[1]}$, which is distinct from the previously discussed 0-form non-invertible symmetry $G_{\text{non-inv}}$ in $\text{QCD}_2(\text{adj})$ [31, 32]. $G_{\text{non-inv}}^{[1]}$ explains why we have infinitely many types of string tensions rather than just N -types from symmetry perspective. Of course, dynamically, this is obvious as the pure Yang-Mills theory does not have charged gluons to screen the adjoint probe charges. The 1-form non-invertible symmetry $G_{\text{non-inv}}^{[1]}$ in pure Yang-Mills is explicitly broken by the introduction of the matter field in adjoint representation down to $\mathbb{Z}_N^{[1]}$ 1-form symmetry. It is an interesting problem how the confining \mathcal{R} dependent strings of pure Yang-Mills theory become confining $k = |\mathcal{R}|$ N -ality dependent strings in massive $\text{QCD}(\text{adj})$.

We can summarize our knowledge about string tension for general $\text{SU}(N)$ theory as follows. Let \mathcal{R} denote a representation of $\text{SU}(N)$ and $k = |\mathcal{R}|$ the N -ality of the representation. Then, the string tensions take the form:

$$\begin{aligned} \sigma_{\mathcal{R}} = 0 & & m = 0 & & \mathbb{Z}_N^{[1]} \text{ broken} \\ \sigma_{\mathcal{R}} = m\lambda^{1/2} \sin\left(\frac{\pi k}{N}\right), & & m \ll \lambda^{1/2} & & \mathbb{Z}_N^{[1]} \text{ unbroken} \\ \sigma_{\mathcal{R}} = \lambda C_{\mathcal{R}} & & m \rightarrow \infty & & G_{\text{non-inv}}^{[1]} \text{ unbroken,} \end{aligned} \quad (2.6)$$

where $C_{\mathcal{R}}$ is quadratic Casimir for representation \mathcal{R} . These theoretical expectations are sketched in Fig. 1. Our simulations may be viewed as probing the properties of the mass-deformed theory, including an extrapolation towards the chiral (i.e. massless) limit.

2.2 Vacuum degeneracy, universes vs. ordinary vacua

We add a few remarks on the vacuum degeneracy of the massless theory. As stated above, the theory has 2^{N-1} fold vacuum degeneracy. However, some peculiarities of these vacua require understanding the distinction between super-selection sectors and a stronger notion, called the “universes”.

For ordinary discrete symmetry breaking in two Euclidean dimensions, domain walls are finite tension configurations connecting the vacua. Consider a 1+1 field theory with a \mathbb{Z}_2 symmetry, and a potential $V(\phi) = \frac{1}{2}(\phi^2 - v^2)^2$. In the broken regime, there are two degenerate vacua on \mathbb{R}^2 , and there exists a field configuration (called a kink) at the interface of the two vacua. A kink can be viewed as a particle in the spectrum of the theory. Now, consider the charge-2 ($q = 2$) Schwinger model. This model has a $(\mathbb{Z}_2)_\chi \times \mathbb{Z}_2^{[1]}$ chiral and 1-form symmetry, with a mixed anomaly in between. Let $\mathcal{O}_\chi(x) \equiv \bar{\psi}_R \psi_L(x)$ denote the chiral fermion bilinear. The mixed anomaly implies that

$$\mathcal{O}_\chi(x)W(C) = e^{2\pi i \text{Link}(C,x)/2}W(C)\mathcal{O}_\chi(x), \quad (2.7)$$

i.e. $\mathcal{O}_\chi(x)$ acts as the local topological operator generating the 1-form symmetry, and it measures the charge associated with the Wilson line. Here, $\text{Link}(C, x)$ is the linking number of x and C . Now, assume $\mathcal{O}_\chi(x)|0\rangle = +|0\rangle$ in one of the vacua. Acting on the $|0\rangle$ with a space-like infinite Wilson line W and using (2.7), one can show that the state $W|0\rangle \equiv |W\rangle$ obeys $\mathcal{O}_\chi(x)|W\rangle = \mathcal{O}_\chi(x)W|0\rangle = -W\mathcal{O}_\chi|0\rangle = -|W\rangle$. This is other chirally broken state. Therefore, $W(C)$ is the boundary between the two chirally broken vacua. This makes the difference compared to ordinary \mathbb{Z}_2 breaking (not involving anomalies) manifest. In the former, the kink is a particle in the spectrum of the theory, a finite tension dynamical domain wall. However, in the second model, the “kink” has a charge, +1 under the $\mathbb{Z}_2^{[1]}$ 1-form symmetry. It is non-dynamical and can only be introduced to the theory as an external probe. In other words, the domain wall in the second theory has infinite tension. In particular, in the first model, if the space is compactified on a circle, $\mathbb{R}_t \times S_L^1$, space-independent saddles $\phi(t)$ represent tunneling and the true ground state is the symmetric superposition, $\frac{1}{\sqrt{2}}(|-a\rangle + |a\rangle)$ separated from anti-symmetric combination by e^{-ML} , where M is domain-wall mass. In the second model, no tunneling exists between the broken vacua even if the theory is compactified. The superselection sectors separated by these stronger criteria are called universes.

QCD₂(adj) has a $\mathbb{Z}_N^{[1]}$ 1-form symmetry, for which the generators are local topological operators $U_s(x)$.⁴ The implication of $G_{\text{non-inv}}$, on the other hand, is that there exist $O(2^{2N})$ *topological line operators* $\alpha(C)$. These two types of operators satisfy

$$U_s(x)\alpha(C) = e^{2\pi i/N}\alpha(C)U_s(x). \quad (2.8)$$

If we act on the vacuum $|0\rangle$ with a topological line, then the state $\alpha|0\rangle$ has a different charge under the 1-form symmetry relative to the original vacuum, i.e. the domain wall connecting the two vacua is charged under $\mathbb{Z}_N^{[1]}$. However, in the QCD₂(adj), there are no fundamentally charged matter fields. Hence, we have to view the vacua with different 1-form symmetry charge as distinct universes.

Physically, these universes can be thought of as the theories on the sector generated from the vacuum by different N -ality probes, for example charges ± 1 at $\mp\infty$, respectively. The algebra (2.8) implies that there are N different types of universes distinguished by their charges under the 1-form symmetry. Since there are 2^{N-1} vacua in the theory, each universe must support multiple degenerate vacua. The number of vacua in each universe $\dim[\mathcal{U}_{N,k}]$ is roughly $2^{N-1}/N$. For example,

⁴Definition of $U_s(x)$: delete the point x from the spacetime, and perform the path integral over gauge fields with holonomy $\text{hol}_C(x) = e^{2\pi i n/N} \mathbf{1}$, $n = 0, 1, \dots, N-1$ for small clockwise circles circulating x . The insertion of the operator $U_s(x)$ is equivalent to performing the path integral with non-trivial 't Hooft magnetic flux sector $n \in \mathbb{Z}_N$.

for $N = 3, 4, 5, 6, 9$, the number of vacua in each universe is given by:

$$\begin{aligned}
N = 3 & \quad \dim[\mathcal{U}_{3,k}] = 2, 1, 1 & \quad \text{for } k = 0, 1, 2 \\
N = 4 & \quad \dim[\mathcal{U}_{4,k}] = 2, 2, 2, 2 & \quad \text{for } k = 0, 1, 2, 3 \\
N = 5 & \quad \dim[\mathcal{U}_{5,k}] = 4, 3, 3, 3, 3 & \quad \text{for } k = 0, 1, 2, 3, 4, \\
N = 6 & \quad \dim[\mathcal{U}_{6,k}] = 6, 5, 5, 6, 5, 5 & \quad \text{for } k = 0, 1, 2, 3, 4, 5 \\
N = 9 & \quad \dim[\mathcal{U}_{9,k}] = 30, 28, 28, 29, 28, 28, 29, 28, 28 & \quad \text{for } k = 0, \dots, 8 \quad (2.9)
\end{aligned}$$

Does lattice formulation possess a microscopic non-invertible symmetry? In our work, we mostly use a lattice formulation with Wilson fermions, neither chiral symmetry, nor $G_{\text{non-inv}}$ are respected. In particular, the Wilson term, $ra\bar{\psi}D^2\psi$, in loops generates an $O(a^0)$ additive mass renormalization for fermions, which introduces the \mathcal{O}_χ operator. It also generates, via tree-level gluon-exchange diagram, a four-fermion operator with a dimensionless effective coupling $c_2 \sim r^2 a^2 g^2$ [7], the \mathcal{O}_2 operator. \mathcal{O}_1 will also be generated because it is not protected by any symmetry. Therefore, the lattice QCD₂(adj) in 2d, is in general a multi-scale problem. In particular, the scale associated with coupling g^2 , and the strong scale Λ_{c_2} associated with c_2 as implied by asymptotic freedom should be particularly important. Within the range of our simulations, we do not see the effects of the induced four-fermion terms, very likely because of the volumes we work with, i.e., as if we have accidental non-invertible symmetry in the IR. Perhaps, due to the logarithmic running of c_2 , $\Lambda_{c_2}^{-1}$ is bigger than the box size, and we do not probe its effects yet. It may be useful to tune the coefficient of these operators as desired from the beginning (for example, to strong coupling) to see the effect of these operators on the dynamics of the theory. We leave this as an interesting open problem.

2.3 On $\mathbb{R} \times S^1$, with periodic and anti-periodic boundary conditions

In order to understand some aspects of center-symmetry in QCD₂(adj) on $\mathbb{R} \times S^1$, we compactify the theory on a circle and study its gauge holonomy potential. In the simulations, we consider both anti-periodic and periodic boundary conditions for fermions, where the former is thermal compactification corresponding to partition function and the latter is circle compactification which corresponds to a $(-1)^F$ graded partition function:

$$\begin{aligned}
Z(L) &= \text{tr}[e^{-LH}], & \text{thermal comp.} \\
\tilde{Z}(L) &= \text{tr}[e^{-LH}(-1)^F] & \text{circle comp.} \quad (2.10)
\end{aligned}$$

In the thermal case, L corresponds to an inverse temperature $1/T$. For periodic compactification, L is not related to temperature. Let us denote the Polyakov loop going around the circle by P . Up to gauge conjugations, it can be written as:

$$P = \text{diag}(e^{i\theta_1}, e^{i\theta_2}, \dots, e^{i\theta_N}), \quad \sum_{i=1}^N \theta_i = 0 \quad (2.11)$$

The holonomy potential can be reliably computed at weak coupling, i.e, at sufficiently small circle $g^2 L^2 \ll 1$. Since the theory does not have bosonic propagating degrees of freedom, the holonomy potential is completely dictated by adjoint fermions.

For periodic (+) and anti-periodic (-) boundary conditions, at one-loop order, the holonomy potential is

$$\begin{aligned}
V_{\text{eff},\pm}(P) &= \frac{m}{L\pi} \sum_{n=1}^{\infty} (\pm 1)^n \frac{K_1(nmL)}{n} |\text{tr}(P^n)|^2 \\
&\xrightarrow{m \rightarrow 0} \frac{1}{\pi L^2} \sum_{n=1}^{\infty} \frac{(\pm 1)^n}{n^2} |\text{tr}(P^n)|^2 \quad (2.12)
\end{aligned}$$

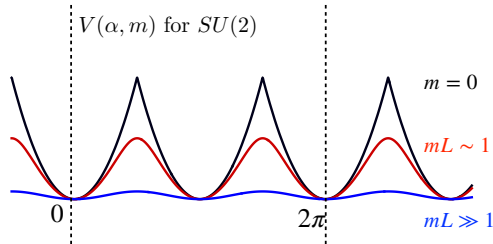


Figure 2: Holonomy potential for $SU(2)$ gauge theory as a function of fermion mass. With increasing mL , the potential flattens. At $m = \infty$, pure Yang-Mills theory in 2d, holonomy potential is zero.

where $K_1(x)$ is modified Bessel function. In the thermal case, the mass-square for Polyakov loop is negative, and at the one-loop order, the \mathbb{Z}_N^0 center-symmetry is spontaneously broken. For the thermal case, we show the mass dependence of the potential in Fig. 2. In particular, since only the matter fields contribute to the potential in two dimensions, the potential flattens with increasing mass of the adjoint fermion, m . Ultimately, at $m = \infty$, pure Yang-Mills theory, $V(P) \rightarrow 0$. In that limit, eigenvalues of the Wilson lines are uniformly distributed.

In thermal case, for generic values of m , the potential has N degenerate minima, given by

$$P_k = e^{i\frac{2\pi k}{N}} \mathbf{1}, \quad \theta_1 = \theta_2 = \dots = \theta_N = \frac{2\pi k}{N} \quad (2.13)$$

We can label these perturbative vacua by $|k\rangle, k = 1, \dots, N$. For $m > 0$, due to tunnelings between the perturbative minima, \mathbb{Z}_N^0 must restore non-perturbatively, as described below. At finite- N and finite m , \mathbb{Z}_N^0 is broken perturbatively, and restored non-perturbatively due to instanton events. Indeed, in the simulations, we will exhibit both these degenerate minima as well as the tunneling events between them.

Remark: Since large- N is a thermodynamic limit, the \mathbb{Z}_N^0 center can break, and indeed, it does so because tunneling rates tends to zero as $e^{-N} \rightarrow 0$. Remarkably, in the present theory, similar to charge- q Schwinger model, the massless limit is extremely interesting. Perhaps, up until a few years ago, we would think that the scenario for the $m > 0$ case should also hold for $m = 0$, at least for odd- N , where there are no fermionic zero modes for Dirac operator [5], and vacuum degeneracy would be lifted because of the instantons. However, the mixed anomaly (between 1-form symmetry and non-invertible symmetry) (2.8) in $\text{QCD}_2(\text{adj})$ and (2.7) (between 1-form symmetry and chiral symmetry) in Schwinger model imply that the transition amplitude between degenerate vacua must be zero. In $\text{QCD}_2(\text{adj})$, this is particularly strange considering that (2.12) is just a bosonic potential with N minima, and there are not robust fermion zero modes for N odd.⁵ But it turns out this is possible. The fact that the transition amplitude can be zero due to destructive interference related to bosonic zero modes has been shown in an explicit example [33]. But the precise way in how the tunneling amplitude must vanish in the context of $\text{QCD}_2(\text{adj})$ has not yet been shown.

⁵An intuitive way to see the non-lifting of degeneracy is as follows. The (2.8) can be satisfied by the $N \times N$ clock C and shift S matrices, $CS = \omega SC$, which act as generators of $\mathbb{Z}_N \times \mathbb{Z}_N$. Since $\mathbb{Z}_N \times \mathbb{Z}_N$ are exact symmetries, the generators must commute with Hamiltonian, $[C, H] = [S, H] = 0$. But the only thing that commutes with both is identity operator, $H = E\mathbf{1}_N$, with exact N -fold degeneracy. Hence, degeneracy cannot be lifted despite the existence of instantons.

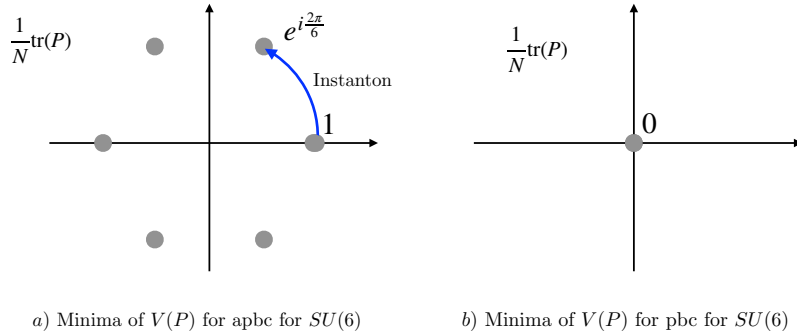


Figure 3: Minima of the holonomy potential a) For fermions endowed with anti-periodic boundary conditions, there are N -minima. b) For fermions endowed with periodic boundary conditions, there is unique minimum.

For the periodic boundary conditions, the mass square for Polyakov loop is always positive, and the minimum of the holonomy potential is unique. It is located at the non-trivial holonomy configuration:

$$P_* = e^{-ia\frac{\pi}{N}} \text{diag} \left(1, e^{i\frac{2\pi}{N}}, e^{i\frac{4\pi}{N}}, \dots, e^{i\frac{2(N-1)\pi}{N}} \right) \quad a = 0, 1 \quad \text{odd, even } N. \quad (2.14)$$

Therefore, the \mathbb{Z}_N^0 is unbroken perturbatively at one-loop order for $m > 0$. For $m = 0$, despite the fact that (2.14) is the minimum of the potential, we should expect subtleties related to mixed anomaly. In the simulations, both (2.13) and (2.14) comes out rather nicely, see Fig. 5.

Analytically, one loses control over the one-loop potential when $gL \gtrsim O(1)$. It is expected that the eigenvalues of the Polyakov loop will be uniformly distributed in that regime with large fluctuations. In simulations, we show this by evaluating the expectation value for the modulus of Polyakov loop, and as well as its susceptibility. In the thermal $\mathbb{R} \times S^1$ set-up, there is a cross-over rather than phase transition at finite- N , but this becomes a genuine phase transition in the $N = \infty$ limit.

2.4 Instantons in the thermal case

As stated above, in the thermal case, there are N -degenerate minima at perturbative level. To describe the tunnelings between them, we consider the 1D quantum mechanical action for the Polyakov loop. To understand the nature of these tunneling events, we can momentarily ignore the fermions, which are gapped due to anti-periodic boundary conditions. The 1D quantum mechanical action is given by

$$S_{1D} = \int dt \left[\frac{1}{2g^2\beta} \sum_{i=1}^N \dot{\theta}_i^2 + \frac{1}{\pi L} \sum_{n=1}^{\infty} \frac{(-1)^n K_1(nLm)}{n^2} \sum_{i,j} \cos n(\theta_i - \theta_j) \right]. \quad (2.15)$$

The perturbative minima of this action is given in (2.13), and we would like to determine the tunneling events. The minimal action configuration interpolating between $|k\rangle$ and $|k+1\rangle$ can be found by using an abelian ansatz for the Polyakov loop

$$P_{\text{ab.an.}} = \text{diag} (e^{i\theta_1}, e^{i\theta_2}, \dots, e^{i\theta_N}) = \text{diag} (e^{i\alpha}, e^{i\alpha}, \dots, e^{-i(N-1)\alpha}) \quad (2.16)$$

In this parametrization, the action takes the form:

$$S_{1D} = \int dt \left[\frac{N^2(N-1)}{2(g^2N)L} \dot{\alpha}^2 + \frac{1}{\pi L} \sum_{n=1}^{\infty} \frac{(-1)^n}{n^2} K_1(nLm) 2(N-1) \cos N\alpha n \right] \\ \xrightarrow{m \rightarrow 0} \frac{N^2(N-1)}{2\lambda L} \int dt \left[\dot{\alpha}^2 + \omega^2 \min_{k \in \mathbb{Z}} \left(\alpha + \frac{2\pi k}{N} \right)^2 \right]. \quad (2.17)$$

where $\omega^2 = \frac{\lambda}{\pi}$. The potential is harmonic and has cusps at $\alpha = \pm \frac{\pi}{N}$ etc. Since the instanton equation is extremely simple, just motion in the periodic extension of the inverted simple harmonic oscillator,

$$\dot{\alpha} = \pm \omega \alpha \quad \text{for } |\alpha| \leq \frac{\pi}{N}, \quad (2.18)$$

the full solution can be found by appropriate patching of the solutions $\exp[\pm \omega t]$.⁶ The configurations interpolating between $\alpha = 0$ ($P = \mathbf{1}$) and $\alpha = \frac{2\pi}{N}$ ($P = \mathbf{1}e^{i\frac{2\pi}{N}}$) are given by

$$\alpha(t) = \frac{2\pi}{N} \Theta(t) - \frac{\pi}{N} \text{Sign}(t) \exp[-\omega|t|] = \begin{cases} \frac{\pi}{N} \exp[\omega t] & t < 0, \\ \frac{2\pi}{N} - \frac{\pi}{N} \exp[-\omega t] & t > 0, \end{cases} \quad (2.19)$$

where $\Theta(t)$ is step function and $\text{Sign}(t)$ is sign function. We set the position moduli of the instanton to zero, $t_0 = 0$. This is a smooth continuous function extrapolating between the two adjacent minima. Its derivative is also continuous with a cusp at $t = 0$, $\dot{\alpha}(t) = \frac{\pi}{N} \omega \exp[-\omega|t|]$. The action of the instanton can be obtained by integrating twice the kinetic term over Euclidean time:

$$S_I = \frac{N^2(N-1)}{2\lambda L} \int dt 2 \dot{\alpha}^2 = (N-1) \frac{\pi^{3/2}}{L\lambda^{1/2}}. \quad (2.20)$$

Therefore, the transition amplitude between adjacent vacua (assuming small non-zero mass for fermions) is approximately given by⁷

$$\langle k+1 | e^{-TH} | k \rangle \sim e^{-(N-1) \frac{\pi^{3/2}}{L\lambda^{1/2}}} \quad (2.21)$$

Two remarks are in order. The instanton action does not scale as $\frac{1}{\lambda} = \frac{1}{g^2N}$, rather it is $\frac{1}{\lambda^{1/2}}$. This is due to the fact that this instanton is induced by the balancing of the classical kinetic term with one-loop potential. i.e. it is some sort of quantum instanton. The second point is the action of the instanton scales as $e^{-N/L}$, hence these tunneling events become forbidden in the large- N limit.

Non-perturbatively, for finite- N and finite m , the degeneracy between the $|k\rangle, k = 1, \dots, N$ states is lifted because of the tunnelings. In the Born-Oppenheimer approximation, the lowest lying N states are

$$|\Psi_q\rangle = \frac{1}{\sqrt{N}} \sum_{k=1}^N e^{i\frac{2\pi k q}{N}} |k\rangle \quad (2.22)$$

⁶We do express the solutions in the $m = 0$ theory to have a sense of the instantons, and their zero mode structure. At $m > 0$, the cusps in the potential and the cusp in $\dot{\alpha}(t)$ smoothen. Moreover, the fermi zero modes will be lifted by soaking them up with the mass operator.

⁷We calculated the instanton action for the holonomy potential at $m = 0$. This action remains the same as long as $mL \ll 1$ at leading order. When $mL \gg 1$, the potential flattens as in Fig. 2, and instantons disappear (or ‘‘melt’’). The strict $m = 0$ limit is more subtle for two reasons. One is that there is a mod 2 index theorem, which indicates $n_L = n_R = 1 \pmod{2}$ zero mode for $N = \text{even}$ and $n_L = n_R = 0 \pmod{2}$ for $N = \text{odd}$. The action of the instanton is still the same, but even if there is no fermi zero modes (as in $N = \text{odd}$), the tunneling must be forbidden because of mixed anomaly between $G_{\text{non-inv}}$ and $\mathbb{Z}_N^{[1]}$ according to (2.8).

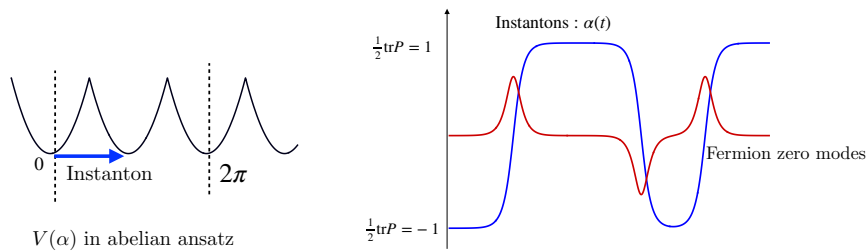


Figure 4: In thermal case, the tunneling between perturbative minima of the holonomy potential is associated with one positive and one negative chirality fermion zero mode for even N . For odd N , these modes are not robust. In the weak coupling semi-classical domain, the chiral condensate receives its contribution from the fermi zero modes localized on instanton. This is also seen in simulations, see Fig.11.

where $|\Psi_0\rangle$ is the ground state. Now, the expectation value of Polyakov loop in the ground state $|\Psi_0\rangle$ vanishes because of the averaging between these N states; while with the periodic boundary conditions, the bosonic potential has a unique center-symmetric minimum,

$$\langle \Psi_0 | \text{tr} P | \Psi_0 \rangle = \frac{1}{N} \sum_{q,k} \langle q | \text{tr} P | k \rangle = \frac{1}{N} \sum_{k=1}^N e^{i \frac{2\pi k}{N}} = 0. \quad (2.23)$$

In other words, Polyakov loop expectation value vanishes because of tunnelings in the high-temperature regime.

In the low temperature, as well as small- L limit of periodic boundary conditions, the reason for its vanishing is that eigenvalues of Polyakov loop are uniformly distributed (as opposed to being clumped), $\frac{1}{N} \text{tr} P_* = 0$.

These two patterns of unbroken center symmetry are physically quite different. In fact, in the large- N limit, which is a way to achieve a thermodynamic limit in the context of quantum mechanics, the center-symmetry breaks even non-perturbatively because the suppressing of tunneling as $e^{-N} \rightarrow 0$. For the periodic boundary conditions, since center-symmetry is unbroken, large- N volume independence must hold similar to 4d QCD(adj) [34]. This implies that the dynamics of QCD₂(adj) at $N \rightarrow \infty$ on \mathbb{R}^2 can be captured by quantum mechanics at small $S^1 \times \mathbb{R}$. While for anti-periodic case, volume independence does not hold, and this theory in the large N limit is expected to have a genuine phase transition at some scale dictated by the strong scale of the theory $T_c \sim \lambda^{1/2}$.

2.5 Chiral symmetry on $\mathbb{R} \times S^1$

Even N , anti-periodic boundary conditions: On $\mathbb{R} \times S^1$ with anti-periodic (thermal) boundary conditions, perturbatively, we have N degenerate minima, with instanton configurations interpolating in between. In this case, there is a mod 2 index theorem for Dirac operator associated with Majorana fermions, which states that number of left/right handed zero modes modulo 2 is a topological invariant. For $N = \text{even}$, there exists only one robust pair of zero modes of opposite chirality, a ψ_+ and a ψ_- , and this can indeed generate a chiral condensate via instanton effects [5]. In the past, it was thought that that the instantons are accompanied with $N - 1$ positive chirality and $N - 1$ negative chirality fermion zero modes [1, 8]. As argued therein, except for $N = 2$, this number is way too large to induce a fermion bilinear condensate in the semi-classical regime. However, as noted above, the mod 2 index theorem resolves this issue for even N [5] (see also [35]).

Below, we will describe what happens in detail for $N = 2$ and comment for general even N . Then, we will discuss odd N case. For even N , in particular $N = 2$, the mixed anomaly between the chiral symmetry and center-symmetry survives,

$$\mathbf{U}_s(x)\mathbf{U}_\chi(C) = (-1)\mathbf{U}_\chi(C)\mathbf{U}_s(x) \quad \text{for even } N. \quad (2.24)$$

We can view large-Wilson loops as the generator of the discrete chiral symmetry, and chiral bilinear $\psi_+\psi_-$ as the generator of the 1-form center-symmetry. Therefore, in the compactified theory, we can express the algebra in terms of Polyakov loops and chiral operator as:

$$\text{tr } \psi_+\psi_- P = (-1)P \text{tr } \psi_+\psi_- \quad \text{for even } N. \quad (2.25)$$

For $N = 2$, the non-invertible symmetry does not play a role, and the story is quite similar to charge- q Schwinger model with $q = 2$ [18–22].

We can describe the states in the two dual bases. One is the eigenbasis $|\ell\rangle$ of the Polyakov loop and the other is the eigenbasis $|\widetilde{m}\rangle$ of the chiral operator. The action of the Polyakov loop and chiral operator in these bases are (still focusing on $\text{SU}(2)$ in the following):

$$\frac{1}{2} \text{tr } P|\ell\rangle = (-1)^\ell|\ell\rangle, \quad \text{tr } \psi_+\psi_-|\ell\rangle = |\ell+1\rangle, \quad \ell = 0, 1 \quad (2.26)$$

$$\text{tr } \psi_+\psi_-|\widetilde{m}\rangle = (-1)^m|\widetilde{m}\rangle, \quad \frac{1}{2} \text{tr } P|\widetilde{m}\rangle = |\widetilde{m}+1\rangle, \quad m = 0, 1. \quad (2.27)$$

As a consequence of the algebra (2.25), the P and $\psi_+\psi_-$ operators cannot be simultaneously diagonalized. A simple transformation relates the two bases:

$$|\widetilde{0}\rangle = \frac{1}{\sqrt{2}}(|0\rangle + |1\rangle), \quad |\widetilde{1}\rangle = \frac{1}{\sqrt{2}}(|0\rangle - |1\rangle). \quad (2.28)$$

In the $m = 0$ case, the tunneling amplitude between the eigenstates of the Polyakov loop $|0\rangle, |1\rangle$ is zero because instantons carry robust fermion zero modes. Reciprocally, the tunneling amplitudes between the eigenstate of the chiral operator $|\widetilde{0}\rangle$ and $|\widetilde{1}\rangle$ is zero because these states are separated by a (non-dynamical) Wilson line and belong to distinct universes. On the \mathbb{R}^2 limit, the would be domain-wall in this theory carries charge-1 under the \mathbb{Z}_2 center-symmetry. But this is not a dynamical degree of freedom in the theory, rather an external probe. This is the reason that $|\widetilde{0}\rangle$ and $|\widetilde{1}\rangle$ are called universes. As a result, we have

$$\langle 1|e^{-TH}|0\rangle = 0, \quad \langle 1|e^{-TH}\mathbf{U}_s|0\rangle \neq 0, \quad (2.29)$$

$$\langle \widetilde{1}|e^{-TH}|\widetilde{0}\rangle = 0, \quad \langle \widetilde{1}|e^{-TH}\mathbf{U}_\chi|\widetilde{0}\rangle \neq 0. \quad (2.30)$$

Although instanton in the basis $|\ell\rangle$ does not lead to tunneling, it causes chiral condensate. As a result, we can express chiral condensate as:

$$\langle \text{tr } \psi_+\psi_- \rangle = \begin{cases} C_1 \frac{1}{L^2\lambda^{1/2}} e^{-(N-1)\frac{\pi^3/2}{L\lambda^{1/2}}} & L\lambda^{1/2} \lesssim 1 \\ C_2\lambda^{1/2} & L\lambda^{1/2} \gg 1. \end{cases} \quad (2.31)$$

The chiral condensate is non-zero at any temperature, but it is exponentially small in the weak coupling semi-classical regime. The lattice results we obtain are nicely consistent with this structure, much smaller at high-temperature than the low-temperature. This is explained in Sec. 3.2, see Fig. 10b.

At high-temperature, our lattice results indicate that the chiral condensate receives dominant contribution from the instanton cores in the semi-classical regime, in accordance with semi-classical

analysis and anomaly structure shown in Fig. 4. See Fig. 11 for instanton profile on the lattice and its contribution to chiral condensate (further details in Sec. 3.2).

For even $N > 2$, we note a few differences without going into details. First of all, the mode 2 index theorem tells us that $n_+ = n_- = 0 \pmod{2}$ for instantons between $|\ell\rangle \rightarrow |\ell + 2\ell'\rangle$ ($\ell' = 1, 2, \dots$), evenly separated tunneling events. This implies that there is no obstruction for the transitions between $|\ell\rangle \rightarrow |\ell + 2\ell'\rangle$ from the fermi zero modes. However, the mixed anomaly between the non-invertible symmetry and center-symmetry (2.8) enforces that the tunneling between $|\ell\rangle \rightarrow |\ell + 2\ell'\rangle$ must also vanish. Hence, the ground state must retain an N -fold degeneracy. If one explicitly breaks the $G_{\text{non-inv}}$ but not ordinary symmetries, then the ground state will be exactly 2-fold degenerate for even N , with the value of the condensate as in (2.31).

Odd N , anti-periodic boundary conditions: For N odd, the mod 2 index theorem indicates that there are no robust fermion zero modes for instantons interpolating between the perturbative vacua $|\ell\rangle$, $\ell = 0, 1, \dots, N-1$. The would-be zero modes of the instanton will be lifted by fluctuations. Therefore, one may expect that the chiral condensate must vanish in the thermally compactified theory. We will show that this is indeed the case. However, in the lattice simulations, we observe a finite condensate. Yet, this is not a contradiction as we explained below, because of subtleties related to cluster decomposition.

We first note one of the remarkable features of the theory. Clearly, the semi-classical potential (2.12) has N minima. But because of the absence of fermi zero modes associated with the instantons interpolating between these vacua, one may reasonably think that vacuum degeneracy ought to be lifted. However, the fact that the mixed anomaly between non-invertible symmetry and 1-form symmetry (2.8) persists in thermal compactification, these degeneracies between vacua cannot be lifted. Therefore, quantum mechanically, N fold degeneracy must survive. This is indeed quite strange, but true. The mechanism through which this may happen is not shown in this work, we expect it to be analogous to the example of the \mathbb{CP}^{N-1} model with winding theta, where degeneracy in a similar situation is not lifted due to subtle effects related to instanton moduli space [33].

Let us work with a specific case, $N = 3$. In this case, on \mathbb{R}^2 , there are $2^{N-1} = 4$ vacua. These 4 vacua are distributed to three universes with charge $q = 0, 1, 2$ sectors as 2, 1, 1. Below, we start with the states as given in Eq. (6.28) of Ref. [3]. These states are in the $\text{QCD}_2(\text{adj})$ in which $(-1)^F : \psi \rightarrow -\psi$ is gauged. This means one works with a generalized partition function in which one sums over spin structures. Ref. [3] refers to the model with gauged $(-1)^F$ as bosonic model and the one it is ungauged as fermionic model. We work with the latter. By undoing $(-1)^F$ gauging, we can move to standard $\text{QCD}(\text{adj})$ in which $(-1)^F$ is a global symmetry. This amounts to identifications $\mathbf{v}_1 \equiv \mathbf{v}_2, \mathbf{v}_3 \equiv \mathbf{v}_4$ in their Eq. (6.28). The states on \mathbb{R}^2 and the expectation value of some operators are therefore given by:

$\langle \mathbf{v}_a \mathcal{O} \mathbf{v}_a \rangle$	\mathcal{U}_0	\mathcal{U}_1	\mathcal{U}_2
\mathcal{O}_A	1	1	1
\mathcal{O}_2	-2	-2	1
\mathcal{O}_χ	$-\sqrt{3}$	$\sqrt{3}$	0

Here, \mathcal{O}_A is the one-form symmetry operator, whose value tells us in which universe we are. \mathcal{O}_2 is 4-fermi operator, and \mathcal{O}_χ is the chiral operator. Clearly, in \mathcal{U}_0 , chiral symmetry is broken.

The degeneracy between the vacuum states of distinct universes cannot be lifted because of anomaly (2.8), but multiple degenerate vacua in a given universe can become non-degenerate with thermal compactification. Let us show how this happens. The degeneracy between the two degenerate vacua in \mathcal{U}_0 gets lifted once the theory is compactified on a thermal circle on $\mathbb{R} \times S^1$. Following the notation of [3], let us denote the two chirally broken vacua by $|\mathbf{v}_1\rangle$ and $|\mathbf{v}_3\rangle$. Since

these are related by spontaneous breaking of an ordinary symmetry with no mixed anomaly with other symmetries, the domain-wall between these two states will be a regular dynamical object. In particular, if we compactify this theory, these two states are able to mix with each other. Therefore, in the theory on $S^1_{\tilde{L}} \times S^1_L$ (compactified on space times Euclidean time), the space-independent configuration interpolating between the two chirally broken vacua is an instanton from the quantum mechanical perspective, with an extensive action proportional to \tilde{L} . Therefore, in the thermally compactified theory, true ground state and first excited states in \mathcal{U}_0 are:

$$|\pm\rangle = \frac{1}{\sqrt{2}}(|\mathbf{v}_1\rangle \pm |\mathbf{v}_3\rangle) \quad (2.32)$$

The energy splitting between $|-\rangle$ and $|+\rangle$ is proportional to $e^{-\tilde{L}g}$ due to tunneling between these two vacua. In both of these $|\pm\rangle$ states, the expectation value of the chiral condensate vanishes,

$$\langle +|\psi_+\psi_-|+\rangle = \frac{1}{2}(\langle \mathbf{v}_1|\psi_+\psi_-|\mathbf{v}_1\rangle + \langle \mathbf{v}_3|\psi_+\psi_-|\mathbf{v}_3\rangle) = \frac{1}{2}(\sqrt{3} - \sqrt{3}) = 0, \quad (2.33)$$

because of the tunnelings. However, note that the tunneling amplitude is vanishing exponentially with volume of the space $e^{-\tilde{L}g}$, consistent with the fact that at $\tilde{L} \rightarrow \infty$ limit, these two vacua becomes two superselection sectors in \mathcal{U}_0 .

In our simulations, we observe a chiral condensate for SU(3) at all temperatures. It is extremely plausible that, at least in the large \tilde{L} limit, our simulation does not tunnel between the two chirally broken vacua as this rate is suppressed by $e^{-\tilde{L}g}$, and also because we have a bare mass preferring one vacuum over the other (which is probably even a stronger effect as we take $\tilde{L} \rightarrow \infty$ limit before we take the chiral limit. Furthermore, it is not the states $|\pm\rangle$ that satisfy cluster decomposition on \mathbb{R}^2 limit, rather it is the states $|\mathbf{v}_1\rangle, |\mathbf{v}_3\rangle$. Therefore, even though formally, the chiral condensate must vanish because of tunnelings as in (2.33), if we turn on a bare mass (which we do), we are essentially forcing the theory to one of the states, say, $|\mathbf{v}_1\rangle$ which satisfies cluster decomposition and for which the condensate is non-zero. With the above considerations, we end up with three vacua, one in each universe in the large- \tilde{L} , large- L regime by the compactification of the theory.

In large- \tilde{L} , but small- L , we found three perturbative vacua (2.13) as well, by performing an analysis for the gauge holonomy potential, labelled by the phases of the trace of Polyakov loop. These two sets of vacua are naturally discrete Fourier transform of one another, as a consequence of mixed anomaly, (2.8).

$$|\ell\rangle = \frac{1}{\sqrt{3}}(|+\rangle + e^{i\frac{2\pi}{3}\ell}|\mathbf{v}_5\rangle + e^{i\frac{4\pi}{3}\ell}|\mathbf{v}_6\rangle) \quad (2.34)$$

At large- L , we can understand the absence of tunneling by the fact that the domain-walls of the theory on \mathbb{R}^2 are non-dynamical and carry non-trivial charge under $\mathbb{Z}_3^{[1]}$ one-form symmetry. Since there are no such charged objects in the theory, we cannot realize these tunneling events dynamically. On the dual eigenbasis $|\ell\rangle$ of the Polyakov loop, the tunnelings must again vanish. However, since the mod 2 index theorem tells us that there are no fermionic zero modes, we expect this to occur because of integration over the instanton moduli space. Certainly, a more in-depth study is needed concerning these general issues for general N .

3 Observables on the lattice

The relevant observables to understand the behaviour of the theory as a function of compactification radius or inverse temperature on $\mathbb{R} \times S^1$ are the Polyakov loop P_L , its modulus, susceptibilities, as well as the chiral condensate $\bar{\psi}\psi$. The volume averaged Polyakov loop is defined as

$$P_L = \frac{1}{NN_x} \sum_x \text{Tr} \left\{ \prod_{t=1}^{N_t} U_1(x, t) \right\}, \quad (3.1)$$

where U_1 are the lattice links in t direction (defining the temperature $T/a = 1/N_t$). However, as stated in the theory discussion, the expectation value of the Polyakov loop vanishes both at high- T (due to tunneling), as well as low- T due to uniform eigenvalue distribution. Therefore, it is also useful to inspect the modulus of the Polyakov loop, as well as its susceptibility which are clearer indicators of the temperature dependence. We also find it useful to examine the scatter plots of trace of Polyakov loops above and below the cross-over temperatures, as well as profiles of the Polyakov loops as a function of the Monte-Carlo time.

The chiral condensate represented here corresponds always to the volume averaged value,

$$- \langle \bar{\psi}\psi \rangle = \langle \frac{1}{N_s N_t} \text{Tr} D_L^{-1} \rangle \quad (3.2)$$

with the lattice Dirac operator D_L . With Wilson fermions the condensate is subject to additive and multiplicative renormalization. However, since the renormalization is temperature independent, the temperature dependence can still be directly observed even from the Wilson-Dirac operator. To determine the zero temperature value of the condensate, we use overlap fermions by reweighting, see Sec. 3.3. These fermions have much better chiral properties.

At finite temperature, the chiral condensate is expected to be non-zero at any temperature, at least for even- N . This is also true for odd- N for a state which would satisfy cluster decomposition at \mathbb{R}^2 limit, but not for symmetric state. See the discussion in the previous section. As shown in (2.31), the chiral condensate is of order of the strong scale of the theory at low temperatures. At high temperatures, it is expected to be exponentially suppressed, and dominated by instanton effects [5, 8].

Susceptibilities are also useful indicators of scales at which the characteristic of an observable changes, and how it changes. For observable O , it can be defined as:

$$\chi_O = \tilde{V}(\langle O^2 \rangle - \langle O \rangle^2), \quad (3.3)$$

where \tilde{V} is N_x for the Polyakov loop or $N_s N_t$ for the chiral condensate. Note that the Polyakov loop susceptibility χ_{PL} refers, unless stated otherwise, to the susceptibility of the modulus of the Polyakov loop.

Some operators in this theory, which are important for later discussions of bound states and parameter tuning are

$$P_\psi = \bar{\psi}\gamma_*\psi, \quad S_\psi = \bar{\psi}\psi. \quad (3.4)$$

As explained Sec. A.2, we can introduce an effective mass m_π based in the operator P_ψ removing the additive mass renormalization of Wilson fermions.

We investigate the string tensions by evaluating the potential between a pair of test quarks as a function of fermion mass. We apply several methods to obtain more reliable estimates as explained in Sec. 3.4. Finally, we also consider the lightest bound states of the theory. First preliminary results are discussed in Sec. 3.5.

3.1 Polyakov loop related observables

In Fig. 5(a), we show the scatterplot of the Polyakov loop of the generated ensemble for SU(6) gauge theory both for anti-periodic and periodic boundary conditions at small $S^1 \times \mathbb{R}$ (corresponding to high-temperature in thermal compactification.) Indeed, the plot shows that real and imaginary part of the Polyakov loop are concentrated in the neighborhood of six distinct phases, along rays in directions given by $e^{i\frac{2\pi k}{6}}$ ($k = 0, 1, \dots, 5$). These are the perturbatively broken vacua found in (2.13). The simulation scans all possibilities of these phases, which correspond to the scanning of all minima of the potential via tunneling events in the analytic formulation. Note that in this case,

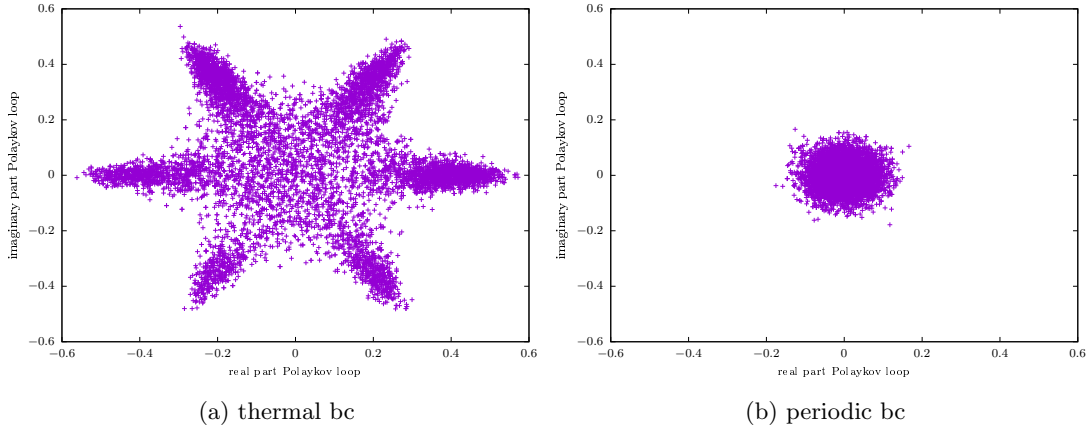


Figure 5: SU(6) QCD₂(adj) on a 4×16 lattice at $\kappa = 0.265$, $\beta = 160$ ($am_\pi = 0.2491(15)$). The distribution of real and imaginary part of the volume averaged Polyakov loop for each configuration is represented in a scatter plot. Polyakov loop for two different fermion boundary conditions at small-circle (high- T) are shown: thermal bc (antiperiodic for fermions) and periodic bc (periodic for all fields). Also note that at large-circle, the scatter plot for both boundary conditions tends towards pattern (b). At small-circle, again the same tendency occurs with increasing the mass of the fermion, as the potential flattens as in Fig. 2.

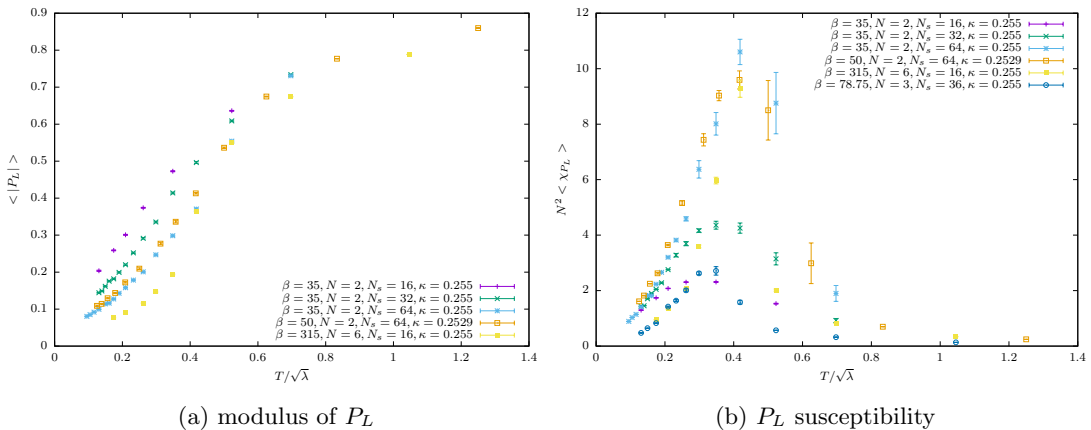


Figure 6: The average modulus and susceptibility of the volume averaged polyakov loop as a function on an $N_t \times N_s$ lattice with thermal boundary conditions for SU(N) QCD₂(adj).

despite the fact that center symmetry is broken perturbatively, it is unbroken non-perturbatively due to instanton events (2.19). For subtleties related to $m = 0$ limit, see the remark in Sec. 2.3.

When the fermions are endowed with periodic boundary condition, in the scatterplot Fig. 5(b), we see a distribution around $P_L = 0$. This implies that \mathbb{Z}_N center-symmetry must remain unbroken at small $S^1 \times \mathbb{R}$, consistent with the theoretical result (2.14) at least for fermion mass $m > 0$. We also note that in the finite-temperature formulation, the scatter plot of the Polyakov loop at low temperatures is essentially identical to Fig. 5b. This provides already an illustrative picture of the transition, but a characterization of its nature requires more detailed analysis of the scaling.

As explained around (2.23), the expectation value of the Polyakov loop is zero even at high temperature, because of the tunneling between the perturbative vacua $\text{tr } P = e^{i \frac{2\pi k}{N}}$. At low temperatures, we expect that the eigenvalues are uniformly distributed, and there, it is the reason for

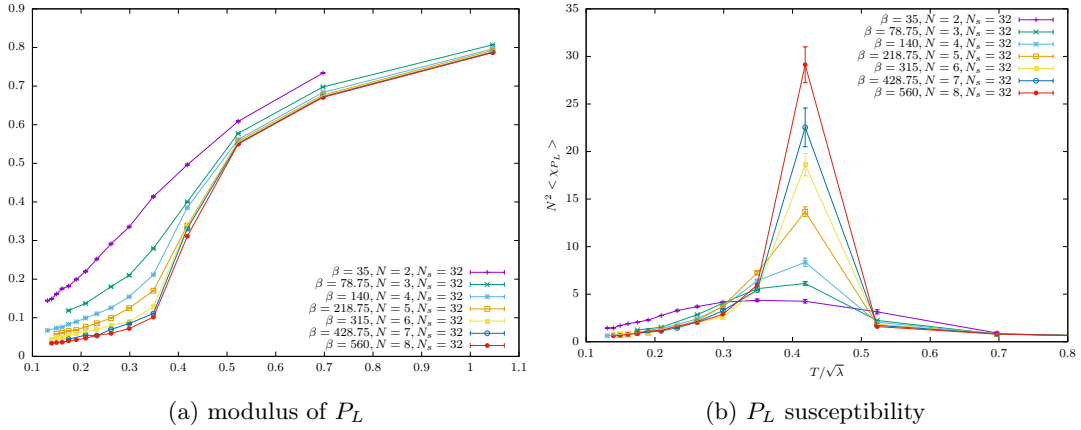


Figure 7: The scaling of the results presented in Fig. 6 with N .

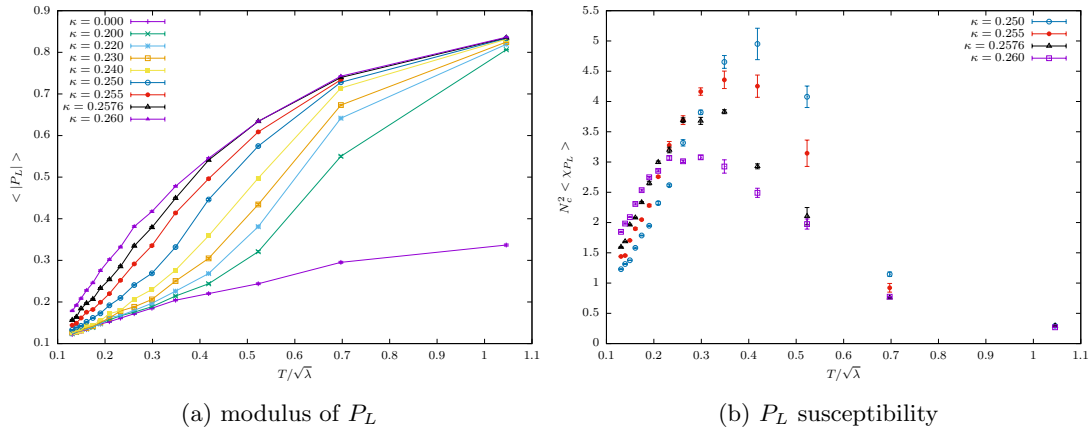


Figure 8: The mass dependence of the transition of the Polyakov line in $SU(2)$ QCD₂(adj) with $N_s = 32$ and $\beta = 35$. In (b) the Polyakov susceptibility for a subset of the masses is shown.

the vanishing of the Polyakov loop. At high temperatures, eigenvalues clump, but then, they can tunnel collectively among vacua. In order to see this effect, it is more useful to inspect modulus of the Polyakov loop. The value of modulus of the Polyakov loop shows a dramatic change from small to large values with the temperature as shown in Fig. 6. A transition point can be identified by the peak of the susceptibility, see Fig. 6b). This behaviour is consistent for different N at fixed temperatures in units of the 't Hooft coupling $\frac{T}{\sqrt{\lambda}} = \frac{1}{N_t} \sqrt{\frac{\beta}{2N^2}}$. The modulus of the Polyakov loop is small at low- T and it is approaching to one at high- T , with an inflection point around $T \sim 0.2, 0.3\sqrt{\lambda}$, where susceptibility reaches to its maximum.

Although the plot of susceptibility has a peak, and the one of the modulus of the Polyakov loop has an inflection point, there is no genuine phase transition here for finite- N in the large N_x limit. The decreasing susceptibility at the highest temperatures and the narrowing of the distribution around the center broken vacua observed at a fixed volume does not indicate a transition in this case. The tunneling probability (2.21) and hence the density of tunneling events scales with $e^{-N/L}$ and is hence reduced at large T but independent of N_x . The effect is rather due to the fact that the average distance of tunneling events increases with the temperature. When it becomes comparable to N_x , the lattice size is not large enough to accommodate enough tunneling events

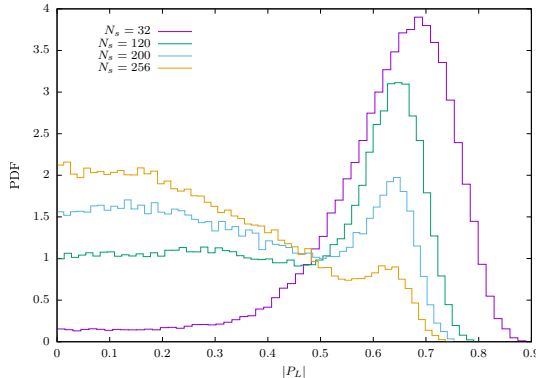


Figure 9: Histogram of the Polyakov loop in $SU(2)$ $QCD_2(\text{adj})$ at $\beta = 35$ and $N_t = 4$ for different N_s .

between the vacua. Going to the thermodynamic limit by increasing N_x , the number of tunnelling events eventually increases, however, linearly since the density is constant. The volume dependence is hence opposite to the usual expectation at a phase transition where tunneling is exponentially suppressed with the volume. In the present case, the tunneling increases at larger volumes and contribution of a deconfined signal in volume averaged observables reduces as shown in Fig. 9. The peak of susceptibility and inflection point can rather be seen as finite- N remnants of the large- N phase transition.

In this theory, a thermodynamic limit can be achieved at large- N , which introduces infinitely many degrees of freedom. Since the tunneling at high- T gets suppressed by $\exp[-(N-1)\frac{\pi^{3/2}T}{\lambda^{1/2}}]$ according to (2.21), the \mathbb{Z}_N center-symmetry breaks spontaneously, as opposed to the finite- N case where tunneling restores it non-perturbatively, and hence, (2.13) are realized as vacua non-perturbatively. Therefore, one obtains a genuine phase transition at large- N limit.

$$\lim_{N \rightarrow \infty} \langle P_L \rangle = \begin{cases} 0 & T < T_c \\ e^{2\pi ik/N} & T > T_c \end{cases} \quad (3.5)$$

Consequently, as shown in Fig. 7, the expected scaling of a phase transition is observed in this limit.

In Fig. 8, we show the mass dependence of the modulus of the Polyakov line over a temperature range. The modulus increases consistently at lower fermion masses. We can understand this from theoretical considerations. In the holonomy potential, increasing the fermion mass, suppresses the potential exponentially. In (2.12), the coefficient of the $|\text{tr } P^n|^2$ is Bessel function of the first kind, $K_1(nLm)$, and for large values of m , it vanishes exponentially, i.e.,

$$K_1(mLn) \rightarrow \sqrt{\frac{\pi}{2mLn}} e^{-nLm}, \quad \text{hence } \lim_{m \rightarrow \infty} V(P) = 0. \quad (3.6)$$

Since the potential is flattened at larger masses, the potential, even at high- T , can no longer pin the holonomy P at the roots of unity $P = e^{i\frac{2\pi k}{N}} \mathbf{1}$. This is sensible because the theory reduces to pure Yang-Mills in the limit, which is almost topological. Hence, even at high- T regime, the eigenvalues start to become uniformly distributed, and $\text{tr } P$ tends towards zero. This is indeed nicely observed in Fig. 8. Similarly, with increasing mass, the gradually flattened effective potential is reflected by a larger maximum susceptibility and the increased density of tunneling events shifts the peak towards higher temperatures.

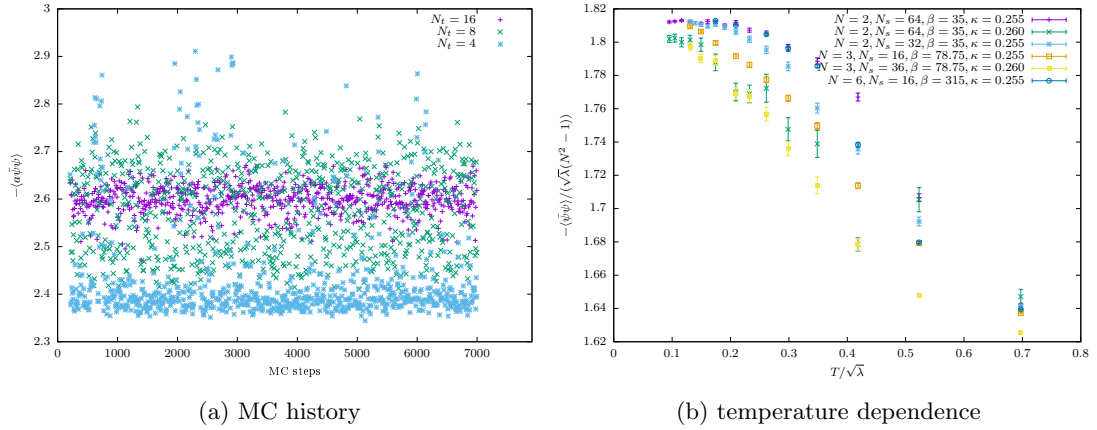


Figure 10: Temperature dependence of bare Wilson fermion condensate. (a) SU(2) QCD₂(adj) on an $N_t \times 32$ lattice, $\kappa = 0.255$, $\beta = 35$. The fermion condensate distribution of the ensembles at different temperatures. (b) The temperature dependence of the average fermion condensate for different masses and N at fixed λ .

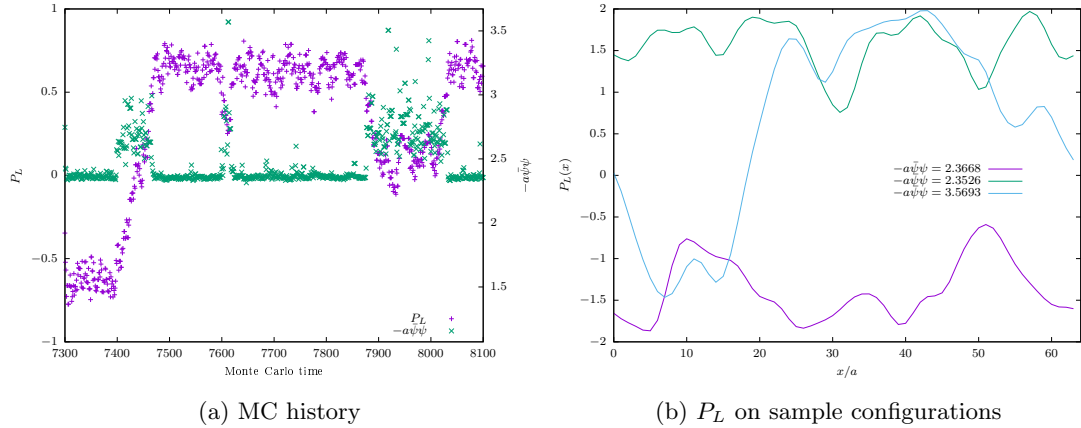


Figure 11: Correlation between Polyakov loop and condensate in QCD₂(adj) (4×64 lattice, $\beta = 35$, $\kappa = 0.260$). (a) The Monte-Carlo history of the Polyakov loop on each configurations is compared to the condensate. (b) The distribution of the Polyakov loop before averaging over L_0 for sample configurations. Gradient flow with Wilson action and flow time $\tau = 2$ has been applied in (b).

3.2 Instantons and chiral condensate at high-temperature

In Fig. 10a, the Monte-Carlo histories of the chiral condensate are shown as a function of temperature. At lower temperature (high- N_t), the value of the condensate is higher, and it starts to fall-off at higher temperature (low- N_t). The temperature dependence of the condensate is shown in Fig. 10b. Although we cannot calculate the chiral condensate analytically in QCD₂(adj), in strong coupling regime, it is worthwhile to point out that Fig. 10b matches very closely to our analytical guess (2.31). It is interesting to note that (2.31) carries main features of the chiral condensate in the Schwinger model as a function of temperature, where in the latter case, it is analytically calculable at any T [21, 36]. In our simulation, note that due to the mentioned large contribution of a small number of configurations, the error is largely underestimated for higher temperatures and smaller fermion masses.

Fig 11 is the counterpart of the instanton analysis at high- T in continuum, shown in Fig. 4. At

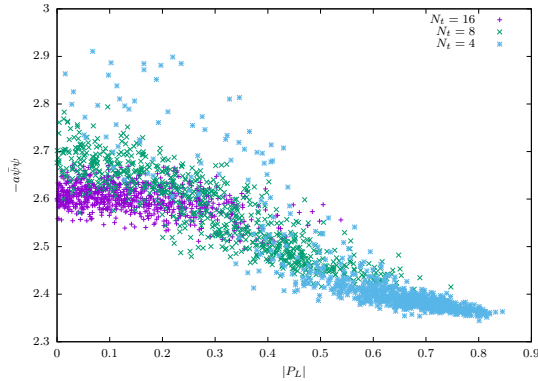


Figure 12: For each configuration the value of the condensate and the Polyakov loop in $\text{QCD}_2(\text{adj})$ are correlated ($N_t \times 32$, $\beta = 35$, $\kappa = 0.255$).

high- T , there are certain configurations which contribute significantly larger values to condensate. As the semiclassical analysis in [5, 8] suggests, the larger values of the condensate are related to configurations where the Polyakov loop, taken as a function of the spacial coordinate x without volume averaging, tunnels between the two adjacent minima of the gauge holonomy potential, see Fig. 4. In continuum, a mod 2 index theorem for the Dirac operator of massless Majorana fermions states that for N even, there is a robust positive chirality and negative chirality fermion zero mode associated with these tunneling events [5]. The density (or number) of these configurations is proportional to instanton fugacity $e^{-S_I} \sim e^{-(N-1)\pi^{3/2}T/\lambda^{1/2}}$ and reduces with increasing temperature. These observations are shown in Fig. 11 which matches nicely with the semi-classical expectations, shown in Fig. 4. We evaluated the temperature dependence of the condensate for $N = 2, 3, 6$, and do not observe a qualitative difference between N -odd and N -even.

Fig. 12 shows the correlation between the chiral condensate and the Polyakov loop. In particular, the chiral condensate is much larger at low- T , where the Polyakov loop is disordered and has large-fluctuations but its volume average is small. The condensate is much smaller at high- T , where the Polyakov loop is pinned at the minima of the holonomy potential and the condensate receives a dominant contribution from a dilute gas of instantons. These instanton contributions are indicated by the scattered points with small volume average Polyakov loop and large condensate.

3.3 Zero temperature fermion condensate

The fermion condensate with Wilson fermion is subject to additive and multiplicative renormalization. The additive renormalization, which makes the interpretation of the zero temperature condensate difficult, is absent with overlap fermions. In our current study, we have not generated ensembles with an overlap operator, but instead we have used reweighting techniques to get the zero temperature condensate. The method based on the complete eigenvalue spectrum of the overlap operator has already been applied in two dimensions for the 't Hooft and Schwinger model. Details are explained in [26]. In this reference the reweighting has been done from pure Yang-Mills theory to the ensemble with overlap fermions. In our case, we have applied the same techniques for a reweighting from Wilson to overlap operator. For that purpose, we have calculated the eigenvalues of the hermitian Dirac-Wilson operator and the overlap operator to obtain the ratio of the Wilson and overlap operator determinants as well as the fermion condensate with the overlap operator.

A meaningful value for the fermion condensate in the chiral (zero mass) limit can only be obtained if the infinite volume limit is taken before the chiral limit. Indeed, the condensate turns to zero if we take the limit of zero fermion mass at a fixed volume. A suitable method is to extrapolate

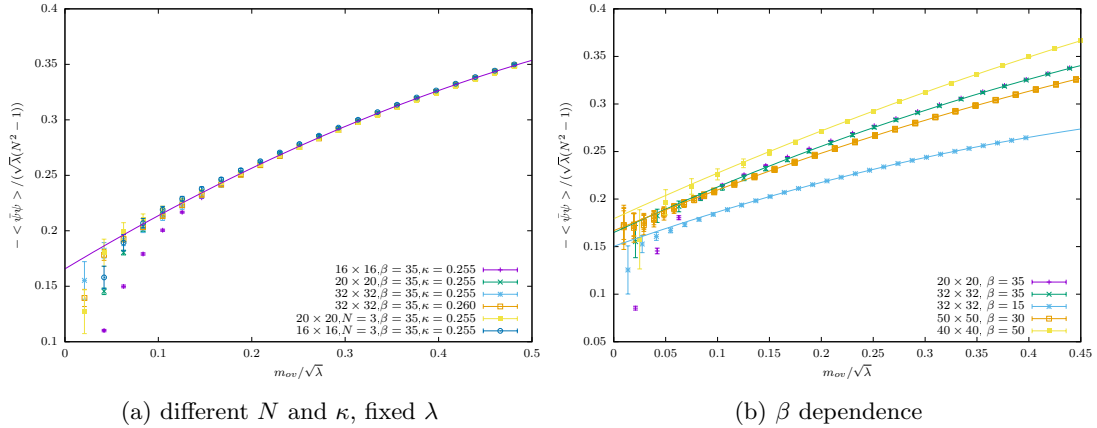


Figure 13: Zero temperature fermion condensate in $\text{QCD}_2(\text{adj})$. The condensate is obtained from a reweighting of Wilson to overlap fermions. The mass m_{ov} corresponds here to the mass in the overlap operator and κ to the value of the mass parameter in underlying Wilson ensemble. A fit up to quadratic order has been used for the chiral extrapolation. (a): At fixed λ , different N , κ , and volumes lead to consistent results. (b): Different β lead to approximately compatible values in the chiral limit.

the condensate to zero fermion mass from a region, in which the results for different volumes are consistent with each other.

The results are presented in Fig. 13. They indicate a finite value of the condensate in the chiral infinite volume limit. The results are independent of the mass parameter (κ) for the underlying Wilson ensemble, but we observe smaller errors at larger κ . With an appropriate scaling, the results of different N are consistent with each other at a fixed 't Hooft coupling. The chiral limit seems to be quite independent of β given the uncertainties of the extrapolation. However, the scaling with the mass parameter m is quite different for the different β and a multiplicative renormalization of the mass parameter appears to be required. It is interesting to note that the fit result in the chiral limit ($-\langle \bar{\psi}\psi \rangle / (\sqrt{\lambda}(N^2 - 1)) = 0.1657(33)$) is close to the Schwinger model ($-\langle \bar{\psi}\psi \rangle / g = 0.15993\dots$) up to a rescaling of $\sqrt{N}(N^2 - 1)$. Note that there is about a factor of two difference with respect the results obtained with a lattice Hamiltonian approach [15].

3.4 String tension

One of our main goals is the investigation of confinement vs. screening scenario from the static quark-antiquark potential and the string tension in the limit of small fermion mass. With this data, we also wish to determine the behavior of the theory in the chiral limit, as $m \rightarrow 0$. In this section we first focus on the case of $\text{SU}(2)$ gauge group and add some remarks about the N dependence in the end.

The static quark-antiquark potential V is obtained from the scaling of the average Wilson loop ($W(\hat{R}_s, \hat{R}_t)$) with its temporal extent R_t and spacial extent R_s (in lattice units $\hat{R}_t = R_t/a$ and $\hat{R}_s = R_s/a$). It can be defined by

$$aV(a\hat{R}_s) = - \lim_{\hat{R}_t \rightarrow \infty} \log(W(\hat{R}_s, \hat{R}_t)) / \hat{R}_t. \quad (3.7)$$

In two dimensional pure Yang-Mills theory, $V(R_s)$ scales linearly with R_s . The simplest ansatz for the scalar potential in two dimensions is therefore $V(R_s) = A + \sigma R_s$. The constant term (A) indicates a possible contribution with perimeter law. In the chiral limit of $\text{QCD}_2(\text{adj})$, the

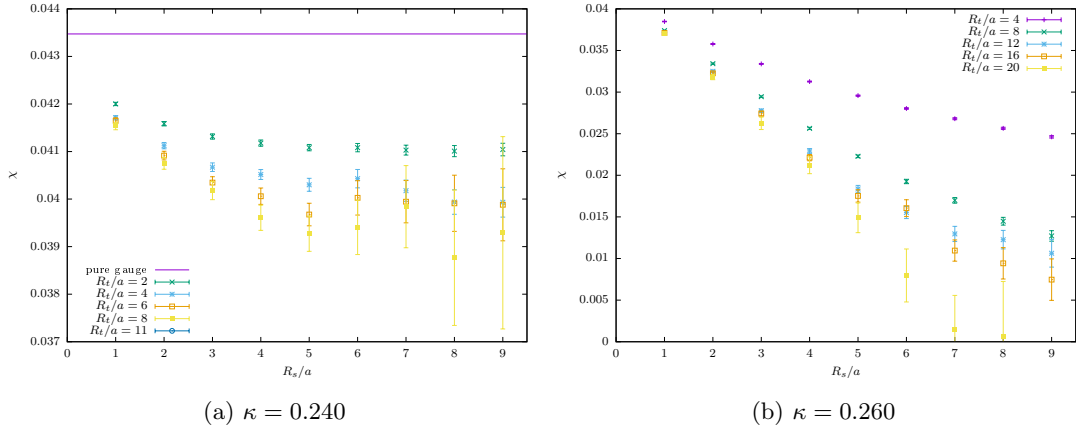


Figure 14: Creutz ratios at two different masses at $\beta = 35$. The smaller κ (larger mass) is simulated on a 24×24 lattice and the larger κ on a 64×64 lattice.

theoretical expectation for SU(2) is screening behaviour [1]: $V(R_s) = c_1(1 - \exp(-c_2 R_s))$. For SU(N), as explained in Sec. 2.1, if non-invertible symmetry is present, we expect a screening behaviour for all representations [3]. If $G_{\text{non-inv}}$ is explicitly broken, we expect a confining potential for all representations, except for N -ality $k = 0, N/2$ [5]. However, if the effects of $G_{\text{non-inv}}$ breaking by the regularization are not relevant at the scales accessible in the simulation, we again expect screening behavior in the massless fermion case. We argue that this is the case for our simulations with Wilson fermions. If we break $(\mathbb{Z}_2)_\chi$ explicitly by turning on a mass deformation, we always expect a confining behaviour. Consequences of these theoretical expectations are illustrated in Fig. 1.

We consider several ways to obtain V or its derivatives in this work. One simple approach is to use Creutz ratios. These correspond to discretised derivatives of $\log(W(R_s, R_t))$ with respect to R_s and R_t ,

$$\chi(\hat{R}_s, \hat{R}_t) = -\log \left(\frac{W(\hat{R}_s, \hat{R}_t)W(\hat{R}_s + 1, \hat{R}_t + 1)}{W(\hat{R}_s + 1, \hat{R}_t)W(\hat{R}_s, \hat{R}_t + 1)} \right). \quad (3.8)$$

If area law holds, χ should approach a plateau at large R_s and R_t . The plateau value corresponds to the string tension.

We have tested this approach for several different parameters. At heavy fermion masses, χ is almost independent of R_s and R_t , but in the low mass regime the string tension seem to decrease towards zero at large distances, see Fig. 14. This may be either an indication of a very small string tension decreasing with $\sigma_k \sim m\lambda$ or potentially a screening behaviour.

Alternatively one can estimate the potential $V(R_s)$ in two different ways from the Wilson loop. It can be approximated from

$$\hat{V}(\hat{R}_s, \hat{R}_t) = \log \left(\frac{W(\hat{R}_s, \hat{R}_t)}{W(\hat{R}_s, \hat{R}_t + 1)} \right), \quad (3.9)$$

either by taking only the largest \hat{R}_t values into account (large R_t method) or by a fit of the \hat{R}_t dependence in order to extrapolate to large \hat{R}_t . The typical way to extrapolate the \hat{R}_t dependence is using the form $\hat{V}(\hat{R}_s, \hat{R}_t) = aV(a\hat{R}_s) + \exp(-d\hat{R}_t)$ in a fit to get $aV(a\hat{R}_s)$ and d . We have implemented both methods, where, in case of the large R_t method, we have averaged the values at the three largest \hat{R}_t values of the measurement. The measurement takes into account only R_s

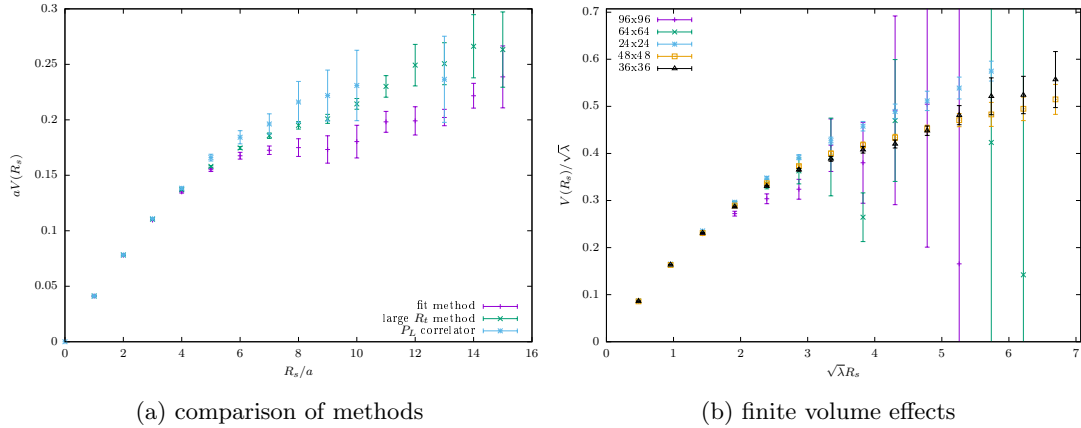


Figure 15: Checks for systematic uncertainties of the static quark-antiquark potential at $\beta = 35$, $\kappa = 0.260$ on a 36×36 lattice comparing different methods and volumes. The differences of the data represent the uncertainties related the estimation of the large R_t limit and finite volume effects.

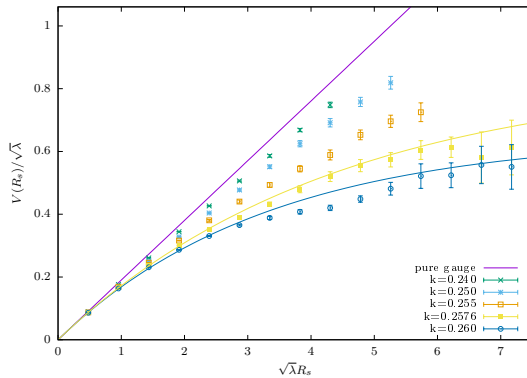


Figure 16: Mass dependence of static quark-antiquark potential at $\beta = 35$ on a 36×36 lattice. This fits of $V(R)$ at the smallest masses are according to $c_1(1 - \exp(-c_2R))$ and the analytic prediction for the pure Yang-Mills case has been added. Results are obtained with the large R_t method.

and R_t values up to half of the lattice size. In some cases we have restricted the data to smaller maximal R_s and R_t values if the signal over noise gets too small.

A further alternative is to estimate $V(R)$ from the correlator of two Polyakov lines at large N_t ,

$$aV(a\hat{R}_s) = -\log(\langle P(0)^\dagger P(\hat{R}_s) \rangle) / N_t. \quad (3.10)$$

We have applied all of the different methods in order to have consistent cross checks of the values and estimate systematic uncertainties. In addition we have also checked the volume dependence. As can be seen in Fig. 15, all of these tests lead to consistent results with some uncertainties at large R_s and relevant finite size corrections only at the smallest volumes and lightest fermion masses. Unless there are large uncertainties at larger R_t , we prefer to focus on the large R_t method since it avoids further assumptions about the R_t dependence. However, it might tend to overestimate $V(R_s)$ at large R_s .

The results for $V(R_s)$ confirm our findings obtained from the Creutz ratios. At large masses a linear raising potential with a string tension slightly smaller than in pure Yang-Mills theory is observed. Decreasing the fermion mass, the slope in the potential drops significantly. For a

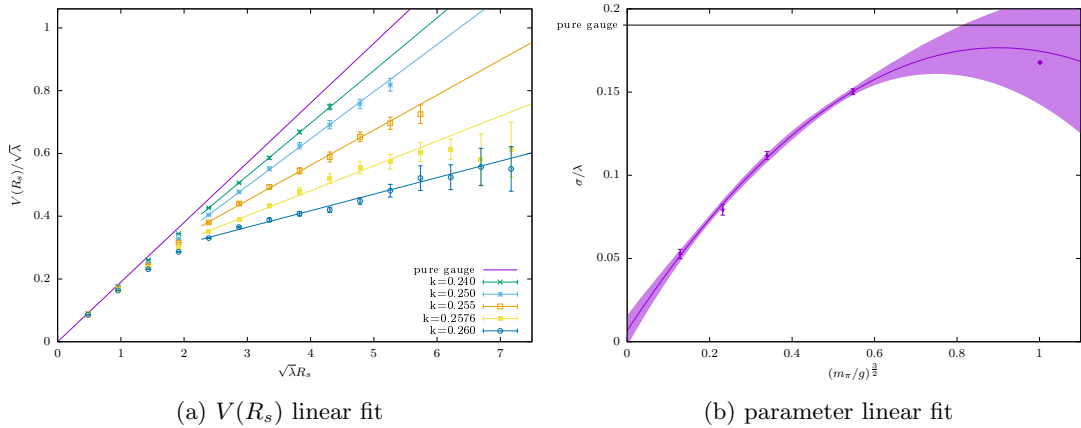


Figure 17: Mass dependence of static quark-antiquark potential like in Fig. 16. (a) $V(R_s)$ at large $\sqrt{\lambda}R_s > 2$ is fitted to the linear dependence $V(R_s) = A + \sigma R_s$. (b) The fit results are extrapolated to the chiral limit using a quadratic polynomial. Similar results are obtained for the gauge group $SU(3)$, see Fig. 22.

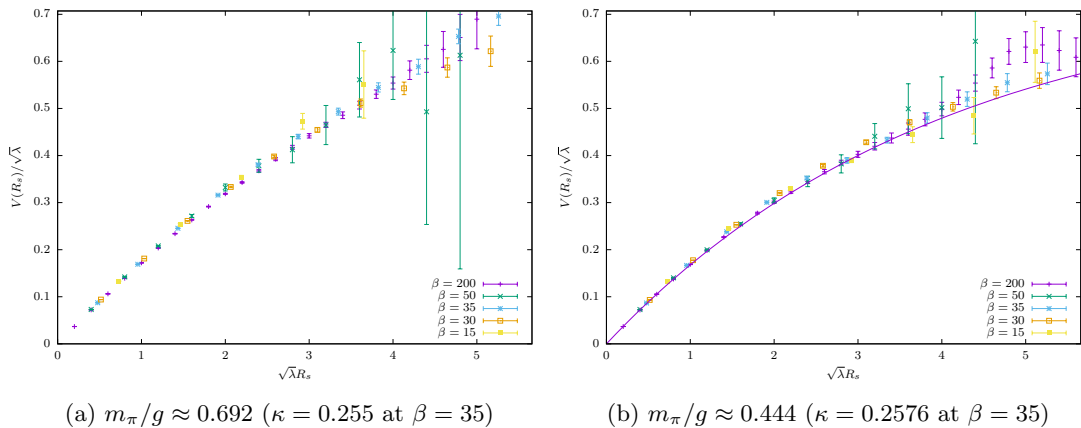


Figure 18: Combined plot of $V(R)$ showing universal behaviour in units of the coupling g . The mass has been fixed to approximately the same value. Different lattice sizes have been combined in this plot: (a) $\beta = 200, 50$: 64×64 ; $\beta = 15, 30$: 36×36 ; $\beta = 35$: 24×24 . (b) $\beta = 200, 50$: 64×64 ; $\beta = 15, 30, 35$: 36×36 . In (b) a fit to $c_1(1 - \exp(-c_2 R_s))$ has been added.

systematic determination of the long distance behaviour, compare Fig. 16 and Fig. 17. In the former, the potential is fitted to a screening potential of the form $c_1(1 - \exp(-c_2 R_s))$, while in the latter, it is fitted to a linear potential at large R_s to obtain the string tension. Theoretically, our expectation for small masses is the one shown in Fig. 17, while at exactly massless point (assuming $G_{\text{non-inv}}$), we expect a screening potential. Indeed, the string tension tends to zero in the chiral limit Fig. 17(b). Note, however, that the linear fit region might move towards larger values of R_s in the chiral limit and the method becomes less reliable. At very small masses, we are not able to distinguish a small string tension from a screening potential.

The remaining step is the extrapolation of the results towards the continuum limit. This can be done by varying β keeping m_π/g fixed. This basically leads to consistent results and not much scaling towards the continuum limit is observed, see Fig. 18.

Towards larger N , the string tension increases at fixed λ and κ , see Fig. 19. The short distance

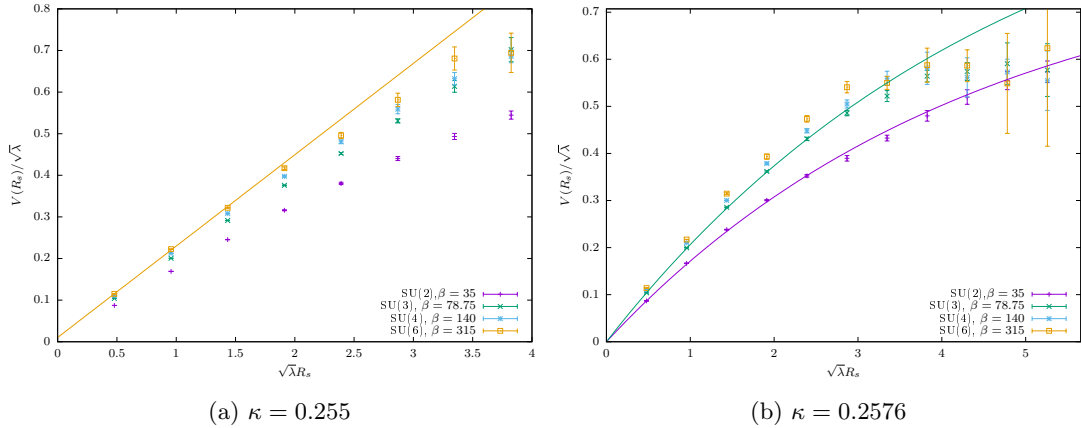


Figure 19: N dependence of $V(R_s)$ at fixed λ and κ . In (a) a linear fit of $V(R_s)$ at $N = 6$; in (b) a fit to $c_1(1 - \exp(-c_2R_s))$ at $N = 3$ and 2 has been added.

β	κ	$m_\pi/\sqrt{\lambda}$	$m_{gg}^2 \frac{\pi}{\lambda}$	$am_S^2 \frac{\pi}{\lambda}$
35	0.25	0.6651(28)	5.52(61)	9.14(41)
35	0.255	0.4859(50)	3.64(58)	7.52(87)
35	0.2576	0.3727(65)	3.4(1.1)	7.10(97)
15	0.255	0.6387(50)	4.45(16)	9.08(45)
15	0.2625	0.4739(31)	3.20(24)	8.69(46)

Table 1: Bound states masses of the gluino-gluon operator (m_{gg}) and the scalar meson (m_S).

$V(R_s)$ shows in general a larger slope than for $N = 2$. However, at the larger distance behaviour at small masses, our simulations cannot distinguish screening from a confining potential with a parametrically small tension.

Recall from theoretical discussion that the theory with exact $G_{\text{non-inv}}$ symmetry is in the deconfined screening phase, and the theory becomes confining if $G_{\text{non-inv}}$ is explicitly broken by either mass operator \mathcal{O}_χ or by the \mathcal{O}_2 operator. The former also breaks the chiral symmetry, but the latter does not. Our current simulation is not at a stage to distinguish these two types of confinement. This stands as an important numerical problem.

3.5 Lightest fermion and boson states

A bosonic state can be formulated in terms of the mesonic scalar operator S_ψ of (3.4). On the lattice, this has to be measured from connected and disconnected fermion contributions similar to the mesons in four-dimensional $\mathcal{N} = 1$ supersymmetric Yang-Mills theory. Consequently the same methods can be applied here, see [37] for further details. In this first investigation, we have just applied a simple stochastic estimation of the disconnected contributions without further smearing or improvements of the operators.

In four-dimensional $\mathcal{N} = 1$ supersymmetric Yang-Mills theory, the fermionic constituent of the supersymmetry bound state multiplet is described by a bound state of fermions and gluons (gluino-gluon) in the following way

$$O_{gg} = \sum_{\mu, \nu} [\gamma_\mu, \gamma_\nu] \text{Tr} [F_{\mu\nu} \lambda] . \quad (3.11)$$

A consistent projection operator onto a state for a correlator in time direction would require the indices μ and ν to run only over spacial indices. This is not possible in two dimensions but

nevertheless the operator has been used in previous studies [29]. In this first study of the theory, we have applied this plain operator as well using a clover definition of the field strength $F_{\mu\nu}$ on the lattice. It is clear that link smearing can not be used to improve the operator and the first three smallest distances of the correlator have to be excluded.

All masses are extracted, as usual, from the exponential decay of the correlators at large distances. The window of the fit is restricted by the small signal to noise ratio at large distances. Our first very rough estimates are shown in Tab. 1. Note that masses for the lightest fermionic and bosonic states have been computed using Discretized Lightcone Quantization and Lattice Hamiltonian approach [13, 15]. The results are around $M^2 \frac{\pi}{\lambda} = 5.7$ for the lightest fermion and $M^2 \frac{\pi}{\lambda} = 10.8$ for the lightest boson. Our data are close to these values, but the systematic uncertainties are currently quite large.

4 Conclusions and future directions

This work aims to initiate a systematic lattice study of $\text{QCD}_2(\text{adj})$, with the hopes of properly understanding this peculiar theory by both theoretical and numerical means. In our lattice formulation, we have used Wilson fermions, which require additive and multiplicative renormalization of the fermion mass. Hence the lattice formulation does not respect the discrete chiral symmetry (which prevents the mass term from being generated), as well as $G_{\text{non-inv}}$ (which prevents the 4-fermion operator \mathcal{O}_2 and mass term from being generated). To obtain chiral condensate in the massless limit, we used overlap fermions by reweighting. Our preliminary results indicate many agreements between theoretical understanding and numerical simulations. But we have not yet explored the realm of more difficult questions concerning the continuum massless theory with $G_{\text{non-inv}}$ symmetry. Below, we summarize our comparison of simulations with theory, and point some problems for future.

With thermal compactification (apbc for fermions), we have numerically investigated the Polyakov loop P , its modulus $|P|$ and susceptibility. At very high-temperatures, we find N possible values, indicating a perturbative breaking of center symmetry. However, for massive fermions, center-symmetry is restored non-perturbatively for finite N . Indeed, in the Polyakov loop scatter plot, we see that the simulation goes through all N minima of holonomy potential, see Fig. 5 for simulations, and Fig. 3 for theory. The modulus of Polyakov loop goes from small values at low temperature to approximately one at high-temperature. Furthermore, the susceptibility makes a peak around $T \sim (0.3 - 0.5)\sqrt{\lambda}$, see Fig. 6. However, it should be emphasized that this is not a phase transition, since $\langle P \rangle = 0$ on both sides. At the large- N limit, we provide evidence that this cross-over becomes a sharp phase transition, see Fig. 7. It should also be pointed out that in a formulation which would respect $G_{\text{non-inv}}$, the N -fold perturbative vacuum degeneracy must survive non-perturbatively because of mixed anomaly (2.8) even at finite- N .

We have investigated chiral condensate numerically for $\text{SU}(2)$, see Fig.10a. It is consistent with theoretical expectations, and in particular, with the instanton result at high-temperature. A rather beautiful result here is Fig. 11, Monte Carlo history of the correlation between the Polyakov loop and condensate, indicating an instanton event in simulation and the fact that chiral condensate receives its dominant contribution from the instanton core. The theoretical counterpart is Fig.4, showing an instanton profile and a fermionic zero modes localized on the instanton core. Fig.12 is also evidence in this direction. We interpret these findings as implications of mixed anomaly between chiral symmetry and center-symmetry of massless theory once it is perturbed by a small mass term. Usually, it is difficult to estimate the chiral condensate with Wilson fermions due to the additive renormalization. In two dimensions it is, however, possible to reweight the Wilson ensembles to the overlap operator. In this way, we have been able to determine the chiral condensate in the zero mass limit as shown in Fig. 13.

We discussed in detail the current theoretical understanding of confinement vs. screening behavior of QCD(adj). The main theoretical result is shown in (2.6) and is plotted in Fig. 1. This understanding is based mainly on three works, [1, 3, 5]. Clearly, this is a hard problem, and depending on whether $G_{\text{non-inv}}$ is explicitly broken or not, the answer changes. Even the exactly massless QCD(adj) confines if 4-fermi operators are added. Our simulations show that the theory in the massless limit tends towards screening behavior. As the fermion mass gets smaller, the tension is reduced in a way proportional to fermion masses, see Fig. 17 and 16. We do not see an indication of 4-fermion induced confinement at the volumes we perform the simulations. Although the Wilson fermions do not respect non-invertible symmetry, the coefficient of the induced 4-fermi operator \mathcal{O}_2 given in (2.3) must be rather small, proportional to $c_2 \sim r^2 a^2 g^2$ [7]. However, c_2 runs according to asymptotic freedom, and ultimately, it will become strong.

There are further steps needed for a more complete analysis of the theory on the lattice. Obviously, the investigations of bound state masses require further improvements using other operators, like the baryonic ones discussed in [38], and better projections to the ground state using smearing. We also plan to extend the data at larger N , which is a thermodynamic limit, which may allow the study of genuine phase transitions, rather than cross-overs. Improvements of the lattice action might be helpful to get a complete picture, in particular using the overlap operator like applied in [39] in four dimensional adjoint QCD. The precise renormalization group scaling and the relevance of four fermion operators requires also further investigations in order to provide a more precise comparison to the results of [3, 5, 7].

Another direction we touched very little, but is important is the simulation of the theory with periodic boundary conditions. In this case, both theory Fig. 3(b) and numerical simulations Fig. 5(b) indicate that a center-symmetric holonomy configuration (2.14) is effective at small- L . Thus, perturbative weak coupling analysis (assuming $m = 0$) indicates that there are $N - 1$ types of massless fermions (living in the Cartan subalgebra) at three level, unlike thermal compactification, where fermions are gapped-out perturbatively by acquiring a thermal mass. Furthermore, periodically compactified (continuum) theory has at least four types of mixed anomalies between the following symmetry pairs $(\mathbb{Z}_N^{[1]}, (\mathbb{Z}_2)_\chi)$, $((\mathbb{Z}_2)_F, (\mathbb{Z}_2)_\chi)$, $((\mathbb{Z}_2)_C, (\mathbb{Z}_2)_\chi)$, and $(\mathbb{Z}_N^{[1]}, G_{\text{non-inv}})$ surviving compactification. Thus, the vacuum structure of the compactified theory is partially explored in [5] and deserves further studies both theoretically (especially concerning the realization of non-invertible symmetry) and numerically. In our preliminary numerical work, we have already seen indications that this may be rather challenging due to zero modes or near-zero modes.

One more direction is performing simulations for different universes. This may have multiple utilities. One is, assuming that $G_{\text{non-inv}}$ emerges at low-energies, then each universe must support exponentially large number of vacua, $\approx 2^{N-1}/N$. It may be interesting to investigate chiral condensates and domain-wall (kink) properties among these vacua, (2.9). The other is related to an order parameter for confinement. To see this, recall that standard partition function $Z(L) = \text{tr}[e^{-LH}]$ sums over different universes without distinguishing them. The insertion of 1-form center symmetry generator $U_s^k(x)$ into the trace turns it into a weighted sum over the universes, $Z_k(L) = \text{tr}[e^{-LH}(U_s)^k] = \sum_{p=0}^{N-1} e^{i\frac{2\pi kp}{N}} \tilde{Z}_p$, where \tilde{Z}_p is the partition function for universe p , and $U_s^k(x)$ measures the charge associated with it (manifested in phase factor in the sum). Here, $k \in \mathbb{Z}_N$ is also equivalent to the insertion of k units of 't Hooft flux, hence Z_k is partition function in 't Hooft flux sector k . Therefore, the partition function for universe- p is given by

$$\tilde{Z}_p = \sum_{k=0}^{N-1} e^{i\frac{2\pi kp}{N}} Z_k \quad (4.1)$$

(4.1) can also be interpreted as gauging the $\mathbb{Z}_N^{[1]}$ 1-form symmetry, which reduces the theory to $SU(N)/\mathbb{Z}_N$ theory. Then, the theory can be probed by test charges (at infinity) in the projective

representation of the $SU(N)/\mathbb{Z}_N$, which corresponds to the discrete theta angle $\theta_p = \frac{2\pi p}{N}$ [40], and \tilde{Z}_p may also be viewed as partition function of $(SU(N)/\mathbb{Z}_N)_p$ theory. In two dimensions, the ratio \tilde{Z}_p/\tilde{Z}_0 is nothing but the ratio of partition functions in the presence of test-charges $\pm p$ at $\pm\infty$ vs. in its absence. Hence, it is naturally an order parameter for confinement. If the ratio scales as $\exp(-\sigma A)$ where A is the area of the Euclidean spacetime, then the theory is confined, otherwise it is deconfined. Hence, it may be useful to study lattice formulations directly projected into these universes.

Acknowledgments

We would like to thank Aleksey Cherman, Theo Jacobson, Yuya Tanizaki, Sahand Seifnashri, Zohar Komargodski, Mendel Nguyen, and Stefan Dürr for useful discussions. M.Ü. is supported by U.S. Department of Energy, Office of Science, Office of Nuclear Physics under Award Number DE-FG02-03ER41260. G. B. is funded by the Deutsche Forschungsgemeinschaft (DFG) under Grant No. 432299911 and 431842497. Some computing time has been provided by the compute cluster ARA of the University of Jena and the compute cluster PALMA of the University of Münster.

A Theory on the lattice

The theory is formulated on a lattice of sizes $L_x = L_0 = aN_x = aN_0$ and $L_t = L_1 = aN_t = aN_1$ with lattice spacing a . In case of non-zero temperature studies, L_t is considered as proportional to the inverse temperature, whereas L_x should be large. If not further specified, the boundary conditions are periodic in all directions, except for the fermion fields, which have antiperiodic boundary conditions in the t -direction. In some cases, we have also investigated periodic fermion boundary conditions. The gauge theory is $SU(N)$. We mainly focus on fermions in the adjoint representation, but our program can handle also fundamental fermions.

A.1 Lattice action and algorithms

The gauge action is represented by a simple plaquette action. We are considering the Wilson fermion action in our main current simulations. In two dimensions, other more involved fermion formulations like fixed point and overlap fermions have been considered. As shown in [26] for the 't Hooft model even a reweighting with the fermion determinant might be feasible⁸. However, in these first simulations, the essential properties of the theory can be investigated already with a simpler fermion action. The Wilson-Dirac operator contains a mass parameter m_0 or, equivalently, the hopping parameter $\kappa = \frac{1}{2(m_0 a + 2)}$. Due to the breaking of chiral symmetry with this fermion action, the mass m_0 gets additive and multiplicative renormalization. The methods to handle the renormalization are well known in four dimensions and we explain some details in Sec. A.2.

The simulations are based on the RHMC algorithm. We have used the program package of our studies of 4D supersymmetric Yang-Mills theory, which has been generalized to enable Monte-Carlo simulations in different dimensions. We have also developed a new independent python package based on tensorflow, capable of simulating these theories [41].

We have tested and verified the code first in the case pure $SU(2)$ Yang-Mills theory in two dimensions. We have also cross checked our results with existing data for two dimensional QCD in fundamental and adjoint representation [42–44].

⁸One difference to the 't Hooft model is, however, that the fermion determinant does not play a role in the large N limit. This is different to the adjoint representation. Hence the scaling of the reweighting factors towards large N is different.

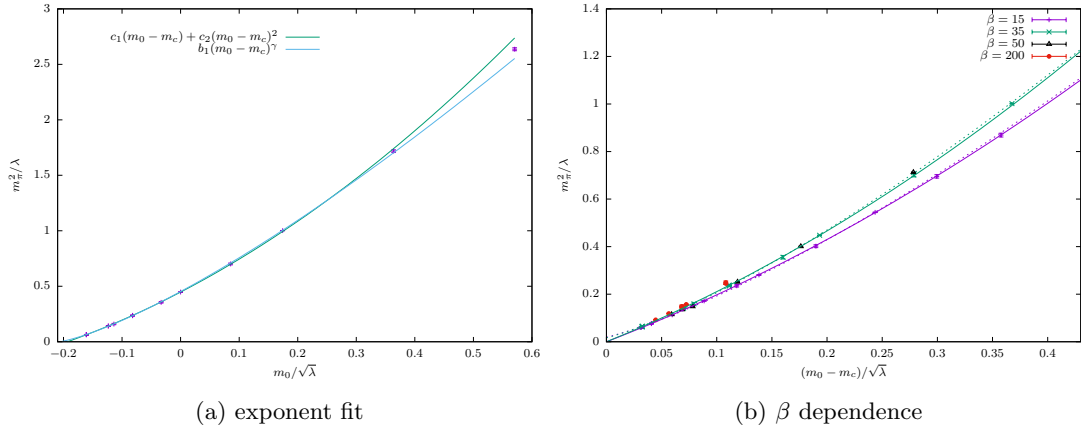


Figure 20: Mass extrapolations in $SU(2)$ $QCD_2(\text{adj})$. Different volumes and gauge couplings are combined in this plot, excluding $Lm_\pi < 3$. (a) The data at $\beta = 35$ is fitted according to a quadratic polynomial (fitting m_c , c_1 , c_2) and with unknown exponent (fitting m_c , b_1 , γ). The first fit result is $m_c/\sqrt{\lambda} = -0.19328(77)$, the second fit $m_c/\sqrt{\lambda} = -0.2084(14)$, $\gamma = 1.311(13)$. (b) The data at $\beta = 35$ and $\beta = 15$ are fitted to a quadratic polynomial. The dashed line corresponds to an additional fit according to $b_1(x - m_c)^{4/3}$. The value of m_c obtained in quadratic fit has been used to shift the data.

A.2 Parameter tuning

The first important step is an identification of the relevant parameter space by choosing the mass parameter ($\kappa = \frac{1}{2(am_0+2)}$) and the gauge coupling ($\beta = \frac{2N}{ag^2}$). In addition the volume dependence has to be considered.

The bare gauge coupling g in two dimensions has the units of mass. All other dimensionful quantities can be expressed in units of the bare gauge coupling. An important dimensionful quantity to quantify the relevant scale of the theory is the string tension. For a first estimate, it can be considered in the pure Yang-Mills limit. The scale of the string tension suggests large values of the gauge coupling if one assumes that the lattice size or lattice spacing in units of the string tension should be similar to common values in four dimensional lattice simulations.

A further hint for the choice of the gauge coupling is the continuum extrapolation. The string tension in units of the gauge coupling can only be extrapolated to a continuum limit value if one excludes large values of g . This is related to the Gross-Witten transition [45]. This transition separates a strong coupling and weak coupling phase at a value $\lambda = 2$ of the 't Hooft coupling $\lambda = g^2N$. This constraint of the gauge coupling are naturally applied in studies of the 't Hooft model [26], but they should also be applied here. It implies a lower limit of the gauge coupling $\beta > N^2$. In order to have an feasible continuum extrapolation, even much larger values of β should be considered. In our $SU(2)$ simulations, we have chosen $\beta = 15, 30, 35, 50, 200$ and as a test considered also $\beta = 3, 6, 10$. Towards larger $SU(N)$, we have tried to stay at constant 't Hooft couplings.

Concerning the values of the mass parameter, there are some difference with respect to the 't Hooft model due to the way the large N limit is taken. Since in the 't Hooft model first the $N \rightarrow \infty$ and then the massless limit has to be considered, the mass in units of the gauge coupling has to be kept at a larger value. In our case, we are interested in the small mass limit even at a fixed N .

In the formulation with Wilson fermions, there is an additive and multiplicative renormalization of the fermion mass. Hence the tuning of the bare mass parameter (m_0 or κ) has to be done. This is usually based on signals for chiral symmetry, which is not a continuous symmetry in this model.

	SU(2)	SU(3)	SU(4)	SU(6)
β	35	78.75	140	315
am_π at $\kappa = 0.255$	0.23239(34)	0.23395(22)	0.23451(99)	0.23457(29)
am_π at $\kappa = 0.2576$	0.18030(55)	0.18155(28)	0.18309(25)	0.18285(43)

Table 2: Comparison of m_π values for different N keeping λ constant.

The situation is quite similar to QCD with one fermion flavour in four dimensions and similar techniques can be applied here. The $a - \pi$ mass (m_π) can be an indication of the chiral limit (corresponding to parameters m_c, κ_c) and the mass tuning. It is derived from the correlator of P in (3.4) by taking only connected fermion diagrams into account. It is not related to a physical state, but it can be considered in a theory with a larger number of adjoint fermions. Our approach follows the techniques of partially quenched chiral perturbation theory used in the four dimensional counterpart. The approximate dependence in four dimensions is provided by partially quenched chiral perturbation theory $m_\pi^2 \propto m$. This means m_c , the value of m_0 at which $m_\pi^2 = 0$, can be linearly extrapolated.

In strong coupling large N limit, the dependence $m_\pi(m_0)$ is known analytically in four dimensions [46]. The same analysis of weak and strong coupling limits provide a possible parameter range for our two dimensional model: $0.25 \leq \kappa_c \leq 0.35$. There might, however, be considerable differences to the four dimensional case. Expanding the strong coupling dependence in powers of m_0 , the second order coefficient has the opposite sign compared to four dimensions, which indicates different corrections to the lowest order chiral extrapolation curve. Investigations of the 't Hooft model have even found a different functional dependence of m_π on m . It has been observed that $m_\pi^2 \propto m$ for $U(N)$, but $m_\pi \propto m^{2/3}$ for $SU(N)$ [26, 47], which is also the expected dependence for the Schwinger model. We have tested different extrapolations with our simulation results as shown in Fig. 20. A fit of the exponent in Fig. 20a yields a value closer to the dependence $m_\pi^2 \propto m^{4/3}$, but a fit with linear dependence and quadratic corrections works equally well. At the current precision, it is therefore not possible to distinguish the two proposals for the mass dependence and the difference is almost negligible in the considered parameter range, see Fig. 20b. In addition we have also checked for possible finite volume effects. Considerable effects for m_π are observed below $Lm_\pi < 3$.

We have considered also larger N keeping the 't Hooft coupling λ fixed. As an example, we have taken $\beta = 35$ at SU(2) as a reference and obtained the results summarized in Tab. 2. This implies that no separate mass tuning is required for different N since the results at fixed λ are consistent.

B Further results

We provide here some additional data to support our findings in the main part of the paper.

In order to show how the pure gauge limit is obtained from the mass dependence, we have added Fig. 21 as an extension of Fig. 8. The peak of the susceptibility moves towards higher temperatures as the mass increases if all other parameters are kept fix. It is expected to scale roughly like a fixed critical mL if the mass is sufficiently heavy, see Eq. (3.6). At temperatures below the peak, the susceptibility decreases with increasing masses, finally approaching the pure gauge limit. This limit can be analytically calculated using (3.3) and eq.14.30 in [30], if the susceptibility of the Polyakov loop is considered instead of the susceptibility of its modulus as in the rest of the paper. The analytic prediction is consistent with our simulation data at $\kappa = 0$, and is shown in Fig. 21.

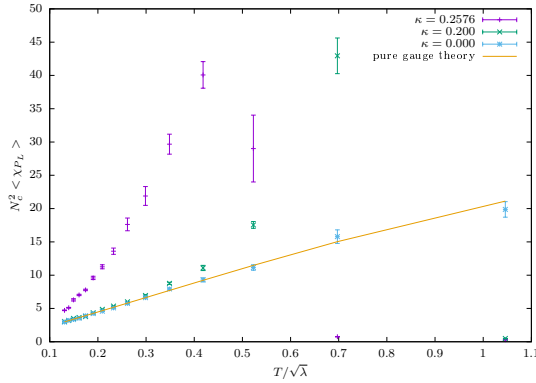


Figure 21: Extension of Fig. 8 with the infinite mass limit, keeping the other parameters fixed. This time showing the susceptibility of the Polyakov loop (not of its modulus). The pure gauge line shows the analytic result. One lower and one heavy mass is added for comparison.

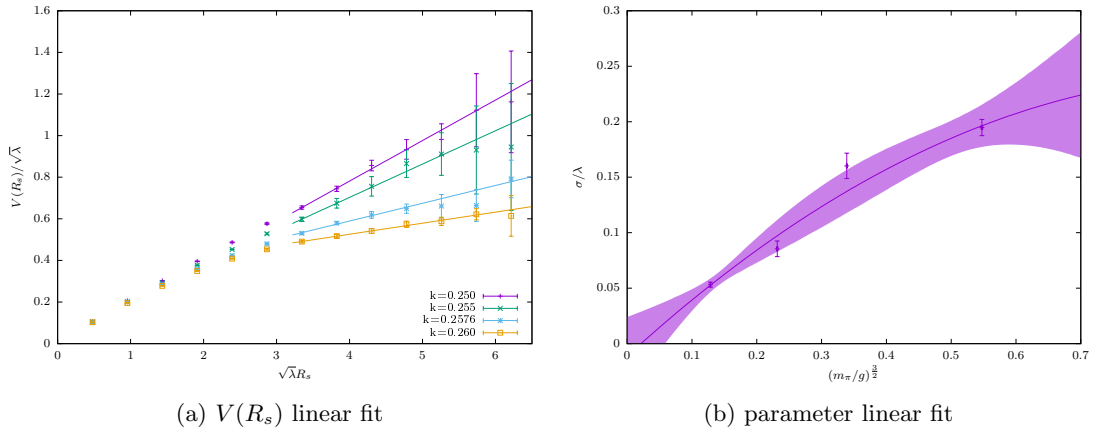


Figure 22: Mass dependence of static quark-antiquark potential like in Fig. 17, this time for the gauge group SU(3). (a) $V(R_s)$ at large $\sqrt{\lambda}R_s > 3.2$ is fitted to the linear dependence $V(R_s) = A + \sigma R_s$. (b) The fit results are extrapolated to the chiral limit using a quadratic polynomial.

The second additional investigation is whether the transition from a confining static potential with significant finite string tension towards screening or near zero string tension in massless limit can be observed for $N \geq 3$. Therefore we repeated the investigation of Fig. 17 for the gauge group SU(3). In pure gauge theory limit as well as at short distances in QCD₂(adj), the slope of the static potential is larger than for SU(2). Therefore a fit of the large distance behaviour has to be done at a larger $\sqrt{\lambda}R_s$. The result is, however, quite consistent with the SU(2) string tension: at zero mass limit, the string tension extrapolates to small values consistent with zero.

References

- [1] D.J. Gross, I.R. Klebanov, A.V. Matytsin and A.V. Smilga, *Screening vs. Confinement in 1+1 Dimensions*, *Nuclear Physics B* **461** (1996) 109.
- [2] M. Ünsal, *Magnetic bion condensation: A New mechanism of confinement and mass gap in four dimensions*, *Phys. Rev. D* **80** (2009) 065001 [0709.3269].

- [3] Z. Komargodski, K. Ohmori, K. Roumpedakis and S. Seifnashri, *Symmetries and Strings of Adjoint QCD₂*, *Journal of High Energy Physics* **03** (2021) 103.
- [4] A.A. Migdal, *Recursion Equations in Gauge Theories*, *Sov. Phys. JETP* **42** (1975) 413.
- [5] A. Cherman, T. Jacobson, Y. Tanizaki and M. Ünsal, *Anomalies, a mod 2 index, and dynamics of 2d adjoint QCD*, *SciPost Physics* **8** (2020) 072.
- [6] D.J. Gross and A. Neveu, *Dynamical Symmetry Breaking in Asymptotically Free Field Theories*, *Phys. Rev. D* **10** (1974) 3235.
- [7] A. Cherman and M. Neuzil, *Beta Functions of 2d Adjoint QCD*, [2401.16604](#).
- [8] A.V. Smilga, *Instantons and fermion condensate in adjoint QCD in two-dimensions*, *Phys.Rev.* **49** (1994) 6836.
- [9] A.V. Smilga, *Two-dimensional instantons with bosonization and physics of adjoint QCD(2)*, *Phys.Rev.* **54** (1996) 7757.
- [10] D. Delmastro, D. Gaiotto and J. Gomis, *Global Anomalies on the Hilbert Space*, *Journal of High Energy Physics* **11** (2021) 142.
- [11] D. Kutasov, *Two Dimensional QCD coupled to Adjoint Matter and String Theory*, *Nuclear Physics B* **414** (1994) 33.
- [12] D. Kutasov and A. Schwimmer, *Universality in two-dimensional gauge theory*, *Nucl. Phys. B* **442** (1995) 447 [[hep-th/9501024](#)].
- [13] R. Dempsey, I.R. Klebanov, L.L. Lin and S.S. Pufu, *Adjoint Majorana QCD₂ at finite N*, *JHEP* **04** (2023) 107.
- [14] U. Trittmann, *Solving two-dimensional adjoint QCD with a basis-function approach*, *Phys. Rev. D* **109** (2024) 016004 [[2307.15212](#)].
- [15] R. Dempsey, I.R. Klebanov, S.S. Pufu and B.T. Søggaard, *Lattice Hamiltonian for Adjoint QCD₂*, [2311.09334](#).
- [16] E. Katz, G. Marques Tavares and Y. Xu, *Solving 2D QCD with an adjoint fermion analytically*, *JHEP* **05** (2014) 143.
- [17] F. Lenz, M.A. Shifman and M. Thies, *Quantum mechanics of the vacuum state in two-dimensional QCD with adjoint fermions*, *Phys. Rev. D* **51** (1995) 7060 [[hep-th/9412113](#)].
- [18] M.M. Anber and E. Poppitz, *Anomaly matching, (axial) Schwinger models, and high-T super Yang-Mills domain walls*, *JHEP* **09** (2018) 076 [[1807.00093](#)].
- [19] M.M. Anber and E. Poppitz, *Domain walls in high-T SU(N) super Yang-Mills theory and QCD(adj)*, *JHEP* **05** (2019) 151 [[1811.10642](#)].
- [20] A. Armoni and S. Sugimoto, *Vacuum structure of charge k two-dimensional QED and dynamics of an anti D-string near an O1-plane*, *JHEP* **03** (2019) 175 [[1812.10064](#)].
- [21] T. Misumi, Y. Tanizaki and M. Ünsal, *Fractional θ angle, 't Hooft anomaly, and quantum instantons in charge-q multi-flavor Schwinger model*, *JHEP* **07** (2019) 018 [[1905.05781](#)].
- [22] M. Honda, E. Itou, Y. Kikuchi and Y. Tanizaki, *Negative string tension of a higher-charge Schwinger model via digital quantum simulation*, *PTEP* **2022** (2022) 033B01 [[2110.14105](#)].
- [23] J.S. Schwinger, *Gauge Invariance and Mass. 2.*, *Phys. Rev.* **128** (1962) 2425.
- [24] A. Cherman, T. Jacobson, M. Shifman, M. Ünsal and A. Vainshtein, *Four-fermion deformations of the massless Schwinger model and confinement*, *JHEP* **01** (2023) 087 [[2203.13156](#)].
- [25] F. Berruto, G. Grignani and P. Sodano, *The Strongly coupled 't Hooft model on the lattice*, *Phys.Rev.D* **62** (2000) 054510.

- [26] F. Berruto, L. Giusti, C. Hoelbling and C. Rebbi, *A Study of the 't Hooft model with the overlap Dirac operator*, *Phys. Rev. D* **65** (2002) 094516.
- [27] P. Korcyl and M. Koren, *Preliminary study of two-dimensional $SU(N)$ Yang-Mills theory with adjoint matter by Hybrid Monte Carlo approach*, *PoS LATTICE2011* (2011) 071 [[1111.4682](#)].
- [28] I. Kanamori and H. Suzuki, *Some physics of the two-dimensional $N = (2,2)$ supersymmetric Yang-Mills theory: Lattice Monte Carlo study*, *Phys. Lett. B* **672** (2009) 307 [[0811.2851](#)].
- [29] D. August, M. Steinhauser, B.H. Wellegehausen and A. Wipf, *Mass spectrum of 2-dimensional $\mathcal{N} = (2, 2)$ super Yang-Mills theory on the lattice*, *JHEP* **01** (2019) 099 [[1802.07797](#)].
- [30] A. Wipf, *Statistical Approach to Quantum Field Theory: An Introduction*, vol. 992 of *Lecture Notes in Physics*, Springer, Heidelberg (10, 2021), [10.1007/978-3-030-83263-6](#).
- [31] M. Nguyen, Y. Tanizaki and M. Ünsal, *Noninvertible 1-form symmetry and Casimir scaling in 2D Yang-Mills theory*, *Phys. Rev. D* **104** (2021) 065003 [[2104.01824](#)].
- [32] T. Pantev and E. Sharpe, *Decomposition and the Gross-Taylor string theory*, *Int. J. Mod. Phys. A* **38** (2023) 2350156 [[2307.08729](#)].
- [33] M. Nguyen, Y. Tanizaki and M. Ünsal, *Winding θ and destructive interference of instantons*, *JHEP* **09** (2023) 033 [[2207.03008](#)].
- [34] P. Kovtun, M. Ünsal and L.G. Yaffe, *Volume independence in large $N(c)$ QCD-like gauge theories*, *JHEP* **06** (2007) 019 [[hep-th/0702021](#)].
- [35] A.V. Smilga, *A comment on instantons and their fermion zero modes in adjoint QCD₂*, *SciPost Phys.* **10** (2021) 152 [[2104.06266](#)].
- [36] I. Sachs and A. Wipf, *Finite temperature Schwinger model*, *Helv. Phys. Acta* **65** (1992) 652 [[1005.1822](#)].
- [37] S. Ali, G. Bergner, H. Gerber, S. Kuberski, I. Montvay, G. Münster et al., *Variational analysis of low-lying states in supersymmetric Yang-Mills theory*, *JHEP* **04** (2019) 150 [[1901.02416](#)].
- [38] S. Ali, G. Bergner, C. Lopez, I. Montvay, G. Münster and S. Piemonte, *Baryonic states in $\mathcal{N} = 1$ supersymmetric $SU(2)$ Yang-Mills theory on the lattice*, *Eur. Phys. J. C* **83** (2023) 558 [[2303.02137](#)].
- [39] G. Bergner, J.C. Lopez, S. Piemonte and I.S. Calero, *Lattice simulations of adjoint QCD with one Dirac overlap fermion*, *Phys. Rev. D* **106** (2022) 094507 [[2205.00792](#)].
- [40] E. Witten, *θ Vacua in Two-dimensional Quantum Chromodynamics*, *Nuovo Cim. A* **51** (1979) 325.
- [41] S. Piemonte, “TfLeonardYM.” <https://github.com/spiemonte/TfLeonardYM>, 2024.
- [42] P. Korcyl, *Solutions of $D = 2$ supersymmetric Yang-Mills quantum mechanics with $SU(N)$ gauge group*, *Journal of Mathematical Physics* **52** (2011) 052105.
- [43] P. Korcyl and M. Koren, *Screening in two-dimensional gauge theories*, *PoS LATTICE2012* (2012) 060.
- [44] D. Bibireata, *Super Yang-Mills theories on the lattice*, Ph.D. thesis, Ohio State U., 2005.
- [45] D.J. Gross and E. Witten, *Possible Third Order Phase Transition in the Large N Lattice Gauge Theory*, *Phys. Rev. D* **21** (1980) 446.
- [46] N. Kawamoto, *Towards the Phase Structure of Euclidean Lattice Gauge Theories with Fermions*, *Nucl. Phys. B* **190** (1981) 617.
- [47] C.J. Hamer, *Lattice Model Calculations for $SU(2)$ Yang-Mills Theory in $(1+1)$ -Dimensions*, *Nucl. Phys. B* **121** (1977) 159.